



## Annual to seasonal glacier mass balance in High Mountain Asia derived from Pleiades stereo images: examples from the Pamir and the Tibetan Plateau

5 Daniel Falaschi<sup>1,2</sup>, Atanu Bhattacharya<sup>3</sup>, Gregoire Guillet<sup>4</sup>, Lei Huang<sup>5</sup>, Owen King<sup>1</sup>, Kriti Mukherjee<sup>6</sup>, Philipp Rastner<sup>7</sup>, Tandong Yao<sup>8</sup>, Tobias Bolch<sup>1</sup>

10 <sup>1</sup>School of Geography and Sustainable Development, University of St Andrews, Irvine Building, North Street St Andrews KY16 9AL, Scotland, UK.

<sup>2</sup>Instituto Argentino de Nivología, Glaciología y Ciencias Ambientales (IANIGLA), CCT-CONICET Mendoza, C.C. 330, 5500 Mendoza, Argentina

<sup>3</sup>Department of Earth Sciences and Remote Sensing, JIS University, Kolkata, India-700109

15 <sup>4</sup>Civil and Environmental Engineering, University of Washington, Seattle, WA, USA

<sup>5</sup>Aerospace Information Research Institute, Chinese Academy of Sciences, Dengzhuang south road 9, Haidian District, Beijing, China-100094

<sup>6</sup>Cranfield Environment Centre, Cranfield University, College Road, Bedford, MK43 0AL, UK

<sup>7</sup>Department of Geography, University of Zurich, Switzerland

20 <sup>8</sup>Institute of Tibet Plateau Research, Chinese Academy of Sciences, Beijing, China

*Correspondence to:* Daniel Falaschi (dfalaschi@mendoza-conicet.gob.ar)

25 **Abstract.** Glaciers are crucial sources of freshwater in particular for the arid lowlands surrounding High Mountain Asia. In order to better constrain glacio-hydrological models, annual, or even better, seasonal information about glacier mass changes is highly beneficial. In this study, we test the suitability of very high-resolution Pleiades DEMs to measure glacier-wide mass balance at annual and seasonal scales in two regions of High Mountain Asia (Muztagh Ata in Eastern Pamir and parts of Western Nyainqêntanglha, South-central Tibetan Plateau), where recent estimates have shown contrasting glacier behavior. We find that the average annual mass balance in Muztagh Ata between 2020 and 2022 was  $-0.11 \pm 0.21$  m w.e. a<sup>-1</sup>, suggesting the continuation of a recent phase of slight mass loss following a prolonged period of balanced mass budgets previously observed. The mean annual mass balance in Western Nyainqêntanglha for the same period was highly negative ( $-0.60 \pm 0.15$  m w.e. a<sup>-1</sup> on average), suggesting increased mass loss rates. The 2022 winter ( $+0.21 \pm 0.24$  m w.e.) and summer ( $-0.31 \pm 0.15$  m w.e.) mass budgets in Muztagh Ata and Western Nyainqêntanglha ( $-0.04 \pm 0.27$  m w.e. [winter];  $-0.66 \pm 0.07$  m w.e. [summer]) suggest winter and summer accumulation-type regimes, respectively. We support our findings by implementing a Sentinel-1–based Glacier Index to identify the firm and wet snow areas on glaciers and characterize accumulation type. The good match between the geodetic and Glacier Index results demonstrates the potential of very high-resolution Pleiades data to monitor mass balance at short time scales and improves our understanding of glacier accumulation regimes across High Mountain Asia.

### 40 1 Introduction

Fluctuations of glaciers across High Mountain Asia are at the core of both scientific and public debate due to their major relevance as sources of freshwater for human consumption, their regulatory role of river runoff, and their contribution to sea level rise (Immerzeel et al. 2020; Vishwakarma et al., 2022; Yao et al., 2022). The combination of varying climatic and accumulation regimes (Yao et al., 2012; Huang et al., 2022), debris-cover fraction (Scherler et al., 2018) glacier surges (Farinotti et al., 2020; King et al., 2021; Guillet et al., 2022), presence of supra-glacial and proglacial lakes (Brun et al. 2019; Maurer et al., 2016; King et al., 2019), and inherent dynamic factors interact with ongoing climate change (Armstrong et al. 2021) and result in spatially and temporally variable mass loss rates (Brun et al. 2019; Dehecq et al., 2019). In recent decades, however, consistent increases in glacier wastage have been observed throughout most of High Mountain Asia (Bhattacharya et al., 2021; Hugonnet et al. 2021). The most notable exception to this trend is the glaciers within the ‘Pamir-Karakorum’ anomaly, which also extends into Eastern Pamir and the Western Kunlun Shan mountains (Kääb et al., 2015; Liang et al., 2022). In this region, glaciers have been in balance or have had slight mass gains since at least the 1970s (Kääb et al., 2015;



55 Bolch et al., 2017, 2019; Brun et al., 2017; Berthier and Brun, 2019). However, recent research hints to an end of this anomaly (Hugonnet et al. 2021; Bhattacharya et al., 2021). Monitoring glacier changes from both remotely-sensed and in situ observations has thus been fundamental for an improved understanding of the relation between climate change and glaciers and has yielded solid evidence of glacier mass loss worldwide (Zemp et al., 2015, Hugonnet et al., 2021). Glacier mass budget is the summation of accumulation and ablation over a specific period of time (Cogley et al., 2011). Presently, the two most widely used methods for determining glacier mass balance are the glaciological and geodetic methods (Cogley, 2009). The glaciological method measures surface mass balance, typically on a seasonal scale, using a combination of conveniently distributed snow pits and stakes to measure accumulation and ablation, respectively (Cogley, 2009). Because of the high costs and logistical constraints involved, less than 0.1% of glaciers spread across the many glacierized mountains in the World have long-term glaciological records that span more than a decade, whilst ~170 glaciers have currently active in situ glaciological mass balance observations (Maussion et al., 2019; WGMs, 2021). On the other hand, the geodetic method consists essentially in the differentiation of multi-temporal and often multi-sourced elevation data (Digital Elevation Models -DEMs), covering usually longer time intervals (>5 years) and larger regions compared to the glaciological method (e.g. Braun et al, 2019; Dussaillant et al., 2019; Shean et al, 2019; Davaze et al., 2020; Hugonnet et al., 2021). In contrast to the glaciological method, the geodetic approach does not only measure the surface mass balance, but also englacial and subglacial processes (Zemp et al., 2013; Andreassen et al., 2016). Moreover, although the glaciological and geodetic methods provide independent observations of glacier mass balance, geodetic surveys of variable temporal resolution can potentially serve to validate and calibrate glaciological records (Zemp et al., 2013; Xu et al., 2018; Wagnon et al., 2021).

75 When shorter time intervals are considered, the geodetic method reveals two fundamental limitations: 1) the DEM precision in relation to the magnitude of the elevation change signal during an annual to seasonal time interval, and 2) the uncertainties of the snow, ice and firn density and densification linked to the volume to mass conversion factor, which are also high over short timescales (Huss, 2013; Pelto et al., 2019). This information is, as noted, only available for a restricted glacier sample worldwide.

80 The increased availability of sub-meter, very-high resolution (VHR) satellite imagery (e.g. Pléiades, WorldView-2) and associated DEMs allows for the quantification of small scale, low magnitude (meter scale) changes at the Earth's surface whilst retaining a suitable level of precision (Berthier et al., 2014). Testing of these DEMs over several mountain sites across the world has confirmed accuracies ranging between 0.2 to 1 m (Berthier et al., 2014; Shean et al., 2016), indicating high potential for assessing glacier elevation changes over short (<3 yrs) time intervals. Glaciers with relatively high mass balance amplitude and heavily snowbound areas are particularly suited to this purpose (Belart et al., 2017, Deshamps-Berger et al., 2020). Additionally, other very-high resolution DEMs can be derived from aerial photographs captured by terrestrial surveys, unmanned aerial vehicles (UAV) and terrestrial or airborne Lidar scanners and laser altimetry (e.g. Ice, Cloud and land Elevation Satellite-2 - ICESat-2) to derive short-term glacier elevation changes (Huss et al., 2013; Fischer et al., 2016; Pelto et al., 2019; Wand et al., 2021; Wu et al., 2022).

90 The major aims of this paper are therefore to investigate the potential and limitations of geodetic mass balance estimates derived from VHR Pleiades satellite data (using 5 DEMs over the 3-year period 2020-2022). We obtain annual and seasonal mass changes in order to make inferences about glacier accumulation regimes in the selected sites based on the geodetic results and by the SAR-derived glacier index of Huang et al (2022), supported by climatic data. For these investigations we have selected two specific regions in High Mountain Asia which have displayed dissimilar mass change rates. The Muztag Ata (Eastern Pamir), which is predominantly influenced by the westerlies and where glaciers have been in a state of mass balance for a longer period, and Western Nyainqentanglha (Central-Eastern Tibet), which is more influenced by the monsoon and has strongly negative mass budgets (Bhattacharya et al. (2021). Moreover, we aim to monitor the ongoing mass balance trends in the Muztag Ata and Western Nyainqentanglha regions.

## 2 Study areas

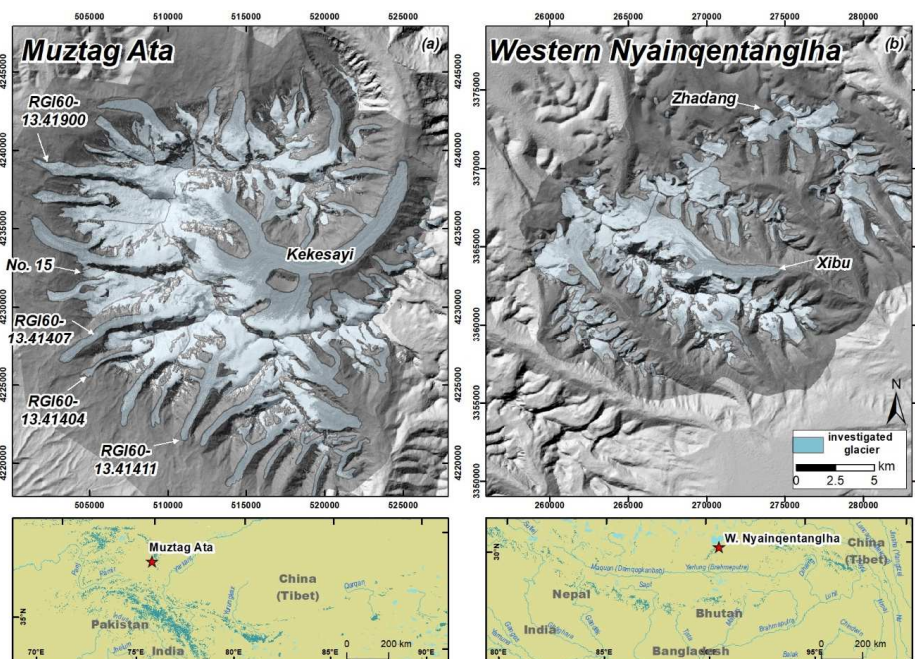
### 2.1 Muztag Ata

105 The Muztag Ata massif (38°17' N, 75°07' E; 7546 m asl.) is situated in Eastern Pamir, west of the Taklamakan Desert (Xinjiang Uighur Autonomous province, China, Fig. 1, left panel). The massif is a result of the exhumation of the Paleozoic metamorphic rocks (along with the nearby Kongur Shan mountains). These peaks represent an area of anomalously high topography at the northwestern tip of the Tibetan Plateau, rising ~4000 m above the ~3500 m asl. Plateau (Seong et al., 2009).

110 A relevant aspect of the atmospheric circulation over High Mountain Asia is its influence on the glaciers' thermal regime. Glaciers in the arid NW Tibetan Plateau are predominantly continental-type, cold-based (with their basal part entirely below the pressure melting point) and receive little precipitation. Climatically, the Muztag Ata region is characterized by a semi-arid continental-type regime, said to be one of the driest and coldest glacierized regions



115 in low- to mid-latitude China (Zhou et al., 2014). Precipitation is mainly driven by the mid-latitude westerly flow  
(Yao et al., 2012) and is concentrated between the spring and summer seasons (April-September). Data from the  
Taxikorgan meteorological station (37°46' N, 75°14' E, ~50 km south of Muztag Ata and placed at ~3100 m asl.),  
collected between 1957-2010, indicates a mean annual temperature of +3.4 °C (Yan et al., 2013; Yang et al.,  
2013). Based on an ice core drilled at ~7000 m, Duan et al. (2015) estimated mean annual snow accumulation of  
120 605 mm w.e.. Glaciers in Muztag Ata represent a relevant water resource on a seasonal to long-term basis,  
regulating the freshwater supply into the Taxikorgan and Gezhe Rivers, tributaries of the Yarkand and Kaxgar  
Rivers respectively, and at the headwater of the Tarim River that runs through the Taklamakan desert (Holzer et  
al., 2015; Zhu et al., 2018a).  
As per the year 2013, the Muztag Ata massif contains ~273 km<sup>2</sup> of glacier ice; the largest individual glacier here  
is Kekesayi Glacier at ~86 km<sup>2</sup> (Holzer et al., 2015). Valley glaciers are cold-based (Zhou et al., 2014), and  
several of them grade distally from debris-free ice into debris-covered and subsequently ice-debris complexes  
similar to the landforms in Central Tien Shan (Bolch et al., 2019). These landforms terminate as ice-cored  
moraines that evidence the presence of buried ice such as thermokarst depressions and a steep front resembling of  
130 intact rock glaciers. In addition, some of these glaciers (RGI60-13.41404, RGI60-13.41407, RGI60-13.41411,  
RGI60-13.41900; Fig.1) currently display behaviour typical of surge-type glaciers (Guillet et al., 2022).  
Previous assessments of glacier mass balance in Muztag Ata (Yao et al., 2012) had detected balanced conditions  
and even slight mass gains in the early 2000's, placing the Muztag Ata area within the Pamir-Karakorum anomaly.  
More recent studies, however, suggest that although glacier area changes are still negligible, the Muztag Ata  
region has recently shifted from approximately balanced conditions to slightly negative glacier mass budgets.  
135 Holzer et al. (2015) and Bhattacharya et al. (2021) found slight mass losses over the last 6 decades (-0.03 m ±0.33  
w.e. a<sup>-1</sup> and -0.06 m ±0.07 w.e. a<sup>-1</sup>, respectively). Extending the time series will allow for the further monitoring  
of this development.



140 **Figure 1.** Overview of the study sites with specific glaciers mentioned throughout the study and location in High  
Mountain Asia. Background images are Pleiades 2019 panchromatic band mosaics overlaid on top of Shuttle Radar  
Topography Mission (SRTM) DEM hillshades.

## 145 2.2 Western Nyainqentanglha

The Western Nyainqentanglha mountains are located in the southeastern center of the Tibetan Plateau. The SW-NE oriented mountain range ~230 km in length reaches a maximum elevation of 7162 m asl. (Mount Nyainqentanglha) (Yao et al., 2010). The main water divide in the Western Nyainqentanglha range drains into the



150 Yangbajain-Damxung valley to the NW and into the Tsangpo-Brahmaputra River (Yao, 2008) further down, and into the Nam Co saltwater lake to the SE. Our study site covers a ~750 km<sup>2</sup> portion situated at the center of the main high mountain range (Fig. 1, right panel).

In general, glaciers to the SE of the Tibetan Plateau are located in a maritime regime under the influence of the Indian summer Monsoon with abundant precipitation. However, the location of the Western Nyainqêntanglha mountains with respect to major atmospheric circulation patterns in High Mountain Asia results in a highly complex climate setting. The NW slopes lie on the windward side of the western winds (which prevail during the dry season), whereas the SE flank is exposed to the easterly winds of the Indian summer Monsoon that dominate in the wet season (Kang et al., 2009). Western Nyainqêntanglha glaciers therefore lie in a transitional zone between the more continental regime to the NW plateau and the maritime regime to the SE, and so polythermal glaciers (mixed basal thermal conditions) are common here (Shi and Menenti, 2013). Overall, the climate around these glaciers has been described as continental summer-precipitation-type, with both accumulation and ablation maxima occurring during the summer months (Kang et al., 2009). The mean annual air temperature at Ambo meteorological station (4820 m asl., ~220 km to the NE of the Nyainqêntanglha range) is -3.0 °C (Bolch et al., 2010). In their energy balance model, Caidong and Sortenberg (2010) estimated the annual precipitation between 700 mm and >900 mm for Xibu Glacier.

160 Bolch et al. (2010) inventoried >1000 individual glaciers covering about 800 km<sup>2</sup> here in 2001, whereas for our specific study site the glacier area accounted for <150 km<sup>2</sup>. The debris-covered Xibu Glacier (~23 km<sup>2</sup>) is the largest sampled glacier. In contrast to the Muztag Ata massif, glaciers in the Western Nyainqêntanglha region have been rapidly shrinking [27% between 1970-2014; Wu et al. (2016)] and losing mass at an accelerated pace (from -0.24 m w.e. a<sup>-1</sup> to -0.47 m w.e. a<sup>-1</sup>) since the 1960's (Zhang and Zhang, 2017; Luo et al., 2020; Ren et al., 2020; Bhattacharya et al., 2021). Both modelled glacier mass balance (-1.0 m w.e. a<sup>-1</sup> for the period 2001 – 2011; Huintjes et al., 2015) and in situ glaciological measurements (-1.2 m w.e. a<sup>-1</sup> to -1.6 m w.e. a<sup>-1</sup> between 2009 and 2014; Zhang et al., 2013 and 2016) on Zhadang Glacier have shown even greater mass loss rates, whilst the in situ mass balance averaged over the 2006-2017 period was of -1.35 m w.e. a<sup>-1</sup> (Yao et al., 2012 and unpublished data).

175

### 3 Data and methods

#### 3.1 Geodetic mass balance

180 To derive annual and seasonal geodetic mass balance estimates, we produced a time series of glacier surface elevation change estimates through DEM differencing. To ensure the robustness of these data, we have considered, and where necessary corrected for, biases related to DEM misalignment, data voids in the elevation change grids, contrasting acquisition dates and seasonal snow conditions. The utilised data and individual processing steps are described in more detail below.

185

##### 3.1.1 DEMs derived from Pléiades tri-stereo imagery

The commercial Pléiades 1A and 1B twin satellites were launched in December 2011 and 2012, respectively. Images are acquired at 0.7 m pixel resolution and delivered by Airbus Intelligence at an oversampled ground sampling distance (GSD) of 0.5 m for the panchromatic band (Gleyzes et al., 2012). In this study, we used Pléiades tri-stereo panchromatic scenes to cover the pre- and post-monsoon seasons in Muztag Ata and Western Nyainqêntanglha between 2019 and 2022 (Table 1). Because of the relatively limited Pléiades footprint of 20 x 20 km (Berthier et al., 2014), both study areas were covered by two or three acquisitions separated in time on most occasions (Table 1). In all cases, partial acquisition dates were no more than 2 weeks apart. From these images, we generated 4 m resolution DEMs and 0.5 m orthoimages using the NASA Ames Stereo Pipeline (ASP, Shean and others, 2016), implementing the Semi-Global-Matching algorithm (Shean et al., 2020).

195 Although no field-surveyed ground control points (GCPs) were used in the DEM extraction process, the vertical bias of Pléiades-derived DEMs with no GCPs has been reported typically between 1-2 m (occasionally up to 7 m) (Berthier et al., 2014; Belart et al., 2017; Falaschi et al., 2022), though this can be reduced to a few decimeters after DEM coregistration. Pléiades DEMs are currently amongst the most common very high resolution DEMs used in geodetic mass balance assessments (e.g. Denzinger et al., 2021; Wagnon et al., 2021; Bhattacharya et al., 2021; Bolch et al., 2022). One of the main advantages of the Pléiades satellites with respect to other sensors used in glaciological applications (e.g. ASTER, SPOT5 HRS, Worldview-1 and Worldview -2), beyond the higher spatial resolution, is that panchromatic bands are coded in a finer 12-bit radiometric resolution, providing a better optical contrast over low contrast and optically saturated areas. Nonetheless, when fresh snow has fallen very shortly before image acquisition (leading to a very high reflection over a large area and lack of contrast in the images), a relatively large number of data voids can be present in the derived DEMs. Such is the case of the



210

September 2021, March 2022 Western Nyainqêntanglha and April 2022 Muztag Ata Pléiades DEMs, where voids account for 20-23% of the glacier area. The remaining DEMs contain less than 9% data voids.

**Table 1.** Acquisition dates of the Pléiades imagery. \*Full area was covered by two scenes acquired on the same day. \*\*Partial coverage only.

Muztag Ata		Western Nyainqêntanglha	
Pléiades	Sentinel-2	Pléiades	Sentinel-2
05-09-2019	03-09-2019	29-10-2019	27-10-2019
11-09-2019	13-09-2019	11-11-2019	11-11-2019
09-09-2020	07-09-2020	08-10-2020*	11-10-2020*
22-09-2020	22-09-2020		
08-09-2021	07-09-2021	30-09-2021**	06-10-2021
21-09-2021	22-09-2021		
22-09-2021			
10-04-2022	10-04-2022	18-03-2022	20-03-2022*
17-04-2022	15-04-2022	19-03-2022	
31-08-2022	02-09-2022	01-11-2022	31-10-2022
27-09-2022	27-09-2022	07-11-2022	05-11-2022

215 **3.1.2 Classification of snow and ice using Sentinel-2 scenes**

The European Copernicus Sentinel-2 satellites (A and B), carrying the MultiSpectral sensor (MSI), were launched in 2015 and 2017. The instruments onboard Sentinel-2A and 2B (swath width = 290 km, orbit repeat rate = 10 days) acquire data in four visible (VIS) and near-infrared (VNIR) bands at 10 m spatial resolution, and six VNIR and short-wave infrared bands (SWIR) at 20 m resolution (Kääb et al., 2016). We used Sentinel-2 imagery to classify surface cover (ice, firn, snow) over Pléiades imagery due to the availability of an automatic, robust method such as ASMAG (Rastner et al., 2019) to identify snow characteristics. Also, the lower spatial resolution and larger swath width (i.e. smaller number of images to be processed) of Sentinel-2 compared to Pléiades are much less demanding from a computational point of view. The distribution of snow, firn and ice surfaces is fundamental for a realistic estimation of annual geodetic glacier mass balance. In this regard, Pelto et al. (2019) judged this distribution to have an even greater impact on geodetic mass changes than snow, firn and ice densities themselves. Whilst snow and bare glacier ice are readily identifiable on multispectral satellite imagery using conventional methods (Paul et al., 2015), the distinction between snow, firn and ice on glacier surfaces can be more difficult. Indeed, several methodological approaches to identify snow line altitudes have shown that firn can be classified as either snow or ice (depending e.g. on the amount of impurities) when using normalized snow indexes or thresholding of single bands/band ratios (e.g. Racoviteanu et al., 2019). Here we implemented the ASMAG algorithm (Rastner et al., 2019, see also Falaschi et al., 2021), using Sentinel-2 images to distinguish between ice and snow/firn areas. In summary, the algorithm converts the raw digital numbers to top of atmosphere reflectance and maps snow cover ratio (SCR). ASMAG then follows the histogram approach of Bippus (2011) applied to a glacier mask to differentiate ice from snow. To this end, it implements an automatic threshold to the near-Infrared (NIR) band, in turn based on the Otsu (1979) thresholding algorithm (Rastner et al., 2019).

We selected Sentinel-2 scenes acquired as close to the Pleiades imagery as possible. Out of 17 images used for the mapping of snow and ice, the acquisition date of only two Sentinel-2 images differed by more than 2 days (see Table 1) from the Pléiades imagery. We inspected ERA5-Land daily temperature and precipitation data to ensure that seasonal snow conditions had not been significantly altered between the Pléiades and corresponding Sentinel-2 scenes (due to snowfall or unusually high temperature events). According to ERA5-Land (Muñoz-Sabater et al., 2021) daily data, there were around 3 cm of fresh snow between the 30 September and 6 October 2021 Pléiades and Sentinel-2 images in the Western Nyainqêntanglha range. Because the 30 September Pleiades scene is anyhow snowbound, the overall seasonal snow conditions appear consistent among the two scenes. As for temperature, the summers of 2019 to 2021 show monthly temperature anomalies below +0.6 °C, which is far below the historical +2.4 °C maximum for the full 1950-2022 series.

Despite the topographic correction featured in the ASMAG algorithm, some glacier parts in cast shadows were initially misclassified as ice in the accumulation regions. To remove these misclassifications, we masked out pixels located above the mean snowline altitude (SLA) plus 2 standard deviations and reassigned them to the snow class and implemented a low-pass filter.

250

**3.1.3 Glacier outlines**



255 We used the glacier outlines of the year 2019 available from Bhattacharya et al. (2021), which were adjusted  
 based on the Randolph Glacier Inventory 6.0 (Randolph Consortium, 2017), as the basis for our glacier inventory.  
 For geodetic mass balance studies of small regional extent, varying quality of glacier polygons may have a  
 relatively large effect on the final results (see e.g. Sommer et al., 2020; Falaschi et al., 2022). Thus, the RGI glacier  
 polygons were manually adjusted (accounting for glacier length changes, removing non-glacierised stable ground,  
 260 reinterpreting debris-covered ice) to fit the glacier extent on each of the Pléiades acquisition dates (Table 1) by  
 visual interpretation of the 0.5 m orthophotos (UTM 43N and 46N for Muztag Ata and Western Nyainqêntanglha,  
 respectively). The glacier area uncertainty was conservatively calculated using the approach followed by Wagnon  
 et al. (2021), as the product of the glacier outline initial perimeter of each sampled time interval and two times the  
 0.5 m ground sampling distance of the Pléiades panchromatic band.

### 265 3.1.4 DEM differencing and generation of elevation change maps

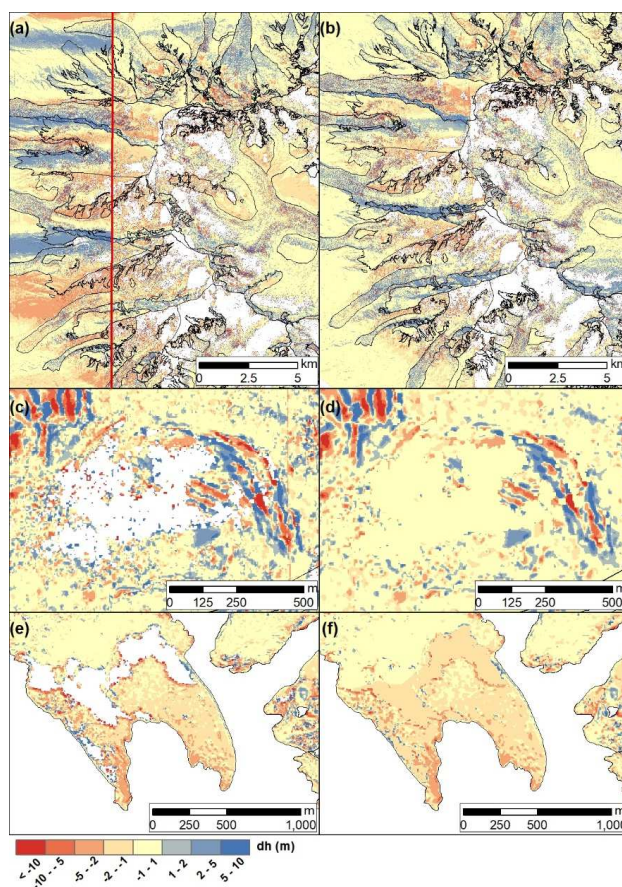
We divided the full 2019–2022 study period into three annual time intervals: 2019–2020; 2020–2021; 2021–2022,  
 and two seasonal (2022 winter and summer) time intervals. Before differencing, we coregistered all DEMs to the  
 reprocessed 2019 Pléiades DEM from Bhattacharya et al. (2021) following Nuth and Kääb (2011). This way, any  
 270 remaining vertical and horizontal shifts between DEMs are minimized before the *dDEM* grids are generated by  
 subtracting the latter from the initial (*reference*) DEMs.

Elevation change grids derived from Pléiades DEMs often show low-frequency biases in off-glacier elevation  
 change residuals (often termed ‘*undulations*,’ Hugonnet et al., 2022), which have been attributed to satellite along-  
 track attitude oscillations [jitter] (Girod et al., 2017; Deschamps-Berger et al., 2020). We implemented the bias  
 275 correction procedure described in Deschamps-Berger et al. (2020) to remove the low-frequency undulation  
 patterns (Fig. 2a, b).

To eliminate on- and off-glacier anomalous cell values from the *dDEM* grids, we considered all values exceeding  
 $\pm 150$  m as outliers and removed them. A second outlier removal step was carried out where the neighboring cells  
 of data gaps in the *dDEM* grids contained high-magnitude elevation differences, which shared statistical  
 280 characteristics with real glacier thinning/thickening. To filter this noise, we first implemented a 3-cell buffer  
 around the data gaps and removed the cells within the buffered areas. We then filled the resulting data gaps using  
 the glacier-wide hypsometric approach of McNabb et al. (2019), fitting a fifth-degree polynomial function to the  
 mean elevation change on 50 m elevation bins (Fig. 2c–f). We chose a 3-cell buffer so as not to remove valid cells  
 from the original *dDEM* grids. Lastly, we mosaiced these tiles to generate the final elevation change maps. Basic  
 285 statistical parameters of our *dDEM* grids (Table 2) after coregistration are akin to previously published geodetic  
 mass balance assessments of annual to seasonal scale in other glacierized regions using Pléiades DEMs (e.g.  
 Beraud et al., 2022).

290 **Table 2.** Statistics of *dDEM* grids on- and off-glacier after coregistration (SD = standard deviation, SE = standard  
 error, NMAD = normalised median absolute deviation).

	Percentage of data voids on- glacier (%)	off-glacier mean elevation difference (m)	off-glacier SD (m)	off-glacier SE (m)	NMAD (m)
<b>Muztag Ata</b>					
2019–2020	8.6	-0.10	2.9	$9.0 \times 10^{-4}$	1.3
2020–2021	10.4	0.06	2.4	$4.8 \times 10^{-4}$	1.3
winter 2022	20.8	0.06	2.9	$6.4 \times 10^{-4}$	1.3
summer 2022	28.1	-0.11	1.7	$3.7 \times 10^{-4}$	1.3
2021–2022	16.4	<0.01	1.9	$4.2 \times 10^{-4}$	1.2
2019–2022	14.4	-0.02	0.7	$4.4 \times 10^{-4}$	1.3
<b>Western Nyainqêntanglha</b>					
2019–2020	6.8	-0.02	1.4	$3.1 \times 10^{-4}$	1.2
2020–2021	23.5	0.03	1.4	$3.7 \times 10^{-4}$	1.1
winter 2022	23.7	-0.11	1.4	$3.7 \times 10^{-4}$	1.0
summer 2022	14.7	0.03	1.0	$2.4 \times 10^{-4}$	0.8
2021–2022	29.7	-0.07	1.0	$2.6 \times 10^{-4}$	0.9
2019–2022	9.2	-0.03	1.0	$2.3 \times 10^{-4}$	0.6



295 **Figure 2.** Along-track bias removal in Muztag Ata *dDEM* grids before (a) and after (b) bias correction. The diverse impact of the jitter effect on individual *dDEM* grids can be appreciated left and right of the red line in panel (a). (c, d) and (e, f) depict examples of outlier removal and gap-filling before and after the implementation of the buffer approach in the Muztag Ata and Western Nyainqentanglha *dDEM* grids, respectively. Note the crevasse motion captured as alternating blue (elevation gain) and red (elevation loss) in the in the Muztag Ata panels.

### 300 3.1.5 Bulk density

Conversion from geodetic volumetric change (in meters) based on the DEM differencing technique to water equivalent (in m w.e.) requires consideration of the densities of the material involved. With no field-surveyed snow density measurements contemporary to our surveyed time periods available, we used the  $410 \pm 60 \text{ kg m}^{-3}$  snow density value used in the energy balance model comprising Muztag Ata N15 and Zhadang glaciers (in Muztag Ata and Western Nyainqentanglha districts, respectively) by Zhu et al. (2018a). According to the authors, this density value was retrieved from snow pits. We assumed a  $\pm 60 \text{ kg m}^{-3}$  uncertainty value, which is a standard value used in geodetic mass balance assessments (Huss., 2013). For glacier ice areas, we used a density of  $900 \text{ kg m}^{-3}$  (Zhu et al., 2018a) and an uncertainty of  $\pm 10 \text{ kg m}^{-3}$  (Clarke et al., 2013).

### 310 3.1.6 Mass balance calculation

We present annual mass balance estimates for the Muztag Ata and Western Nyainqentanglha regions starting in the winter of 2019 up to the summer of 2022 but provide also estimates of the 2022 winter and summer seasons. The annual mass balance  $B_a$  can be defined as the algebraic sum of the winter  $B_w$  and summer  $B_s$  balances



$$B_a = B_w + B_s \quad (1)$$

320 The total volume change  $\Delta v$  ( $\text{m}^3$ ) over a given time interval  $t$  is then derived from the respective elevation difference  $dh$  of the two grids at pixel  $k$  with cell size  $r$  of the DEMs, summed over the number of pixels covering the glacier, and is expressed as (cf. Zemp et al., 2013):

$$\Delta v = r^2 \times \sum dh_i \quad (2)$$

325 Applying the snow and ice masks described in Sect. 4.3, we then assessed the annual and seasonal geodetic mass balance  $\Delta m$  ( $\text{m w.e.}$ ) considering the volume change  $\Delta v$ , the density of the involved material  $\rho$ , and both the snow and ice areas  $A_i$

$$\Delta m = \sum \frac{\Delta v \times \rho}{A_i} \times t^{-1} \quad (3)$$

### 330 3.1.7 Firn densification correction

Lowering of the annual snowpack on glaciers occurs as a result of firn densification, a process that leads to underestimated volume changes (Sold et al., 2013) and is often neglected in geodetic mass balance studies relying on the dDEM technique. We implemented a simple firn densification approach following Sold et al. (2013) to  
335 estimate the annual elevation change due to firn densification  $dh_{\text{firn}}$  integrated over the entire firn column

$$dh_{\text{firn}} = \frac{b_n}{\rho_{\text{firn}_u}} - \frac{b_n}{\rho_{\text{firn}_l}} \quad (4)$$

340 where  $b_n$  is the net mass balance averaged over the previous mass balance year or period (in  $\text{kg m}^{-2}$ ) over the accumulation area [positive, by definition] (Belart et al., 2017).  $\rho_{\text{firn}_u}$  and  $\rho_{\text{firn}_l}$  are the density values at the upper and lower ends of the firn column, set to  $\rho_{\text{firn}_u} = 470 \text{ kg m}^{-3}$  and  $\rho_{\text{firn}_l} = 857 \text{ kg m}^{-3}$ , as retrieved from a 41 m-deep ice core drilled at  $\sim 7000 \text{ m}$  on Muztag Ata (Duan et al., 2015).

Because some of our Pléiades imagery was acquired around the end of the accumulation season (Western Nyainqêntanglha) or contains seasonal snow (Muztag Ata), ‘snow’ areas do not exactly match “accumulation”  
345 areas and can have an overall negative elevation change.

Using the most recent elevation grids available from Bhattacharya et al. (2021) [Muztag Ata: 2013-2019; Western Nyainqêntanglha: 2018-2019] in combination with the “snow” areas derived from the 2019 Sentinel-2 scenes to calculate the net mass balance in the “accumulation” area leads to a negative signal. In consequence, we considered  $b_n$  to be the net mass balance of the snow areas as depicted in the September 2021 (Muztag Ata) and  
350 October 2020 (Western) Pléiades scenes, which are those showing the least amount of seasonal snow, and thus snow areas should be representative of accumulation areas. Although topoclimatic factors can make firn lines vary spatially and temporally (Guo et al., 2014) through time, for the sake of simplicity we assumed that firn densification did not change over different time periods. Our approach is also based on the accumulation rate retrieved from a single year on each study site, whilst some variability is naturally expected (Duan et al., 2015).  
355 We then scaled the firn densification correction linearly according to the length of each time span between consecutive imagery acquisition.

Because of the simplifications and assumptions of the firn correction (equal net accumulation through the study period, constant densification rate through the hydrological year), we considered a 50% uncertainty in the firn correction when quantifying the total mass balance error.  
360

### 3.1.8 Seasonal correction

Ideally, mass balance observations should be made repeatedly at the end of the ablation season to ensure that the full, annual budget of ablation and accumulation has been captured, although data availability means this is rarely  
365 the case. Correction for the impact of such seasonal bias is therefore commonly required (Belart et al., 2017 and 2019; Abdel Jaber et al., 2019).

Neglecting such seasonality corrections can introduce potential biases, since the effect of seasonal signals are particularly strong when short time intervals are considered. A simple approach to account for the seasonal shift of acquired remotely-sensed data with respect to the hydrological cycle consists of using the daily mass balance  
370 rate for the given period to fill in the deficit of missing days or subtract the input of excess days (Abdel Jaber et al., 2019). The extent of the seasonal bias introduced when using this method therefore depends on the fraction of missing or excess days in relation to the onset of the accumulation and ablation periods. We nevertheless chose





375 this approach since our study sites lie in transitional to continental semi-arid environments, where contrary to  
 glaciers in maritime regions, large annual mass balance turnover is not to be expected (Duan et al., 2015; Zhu et  
 al., 2015 and 2018a). Moreover, the percentage of missing/excess days relative to the start of the winter (1 October)  
 and summer (1 April) seasons was below 10% for our Pléiades imagery. We considered that any remaining  
 seasonality-related biases should be within the overall uncertainty range.

### 3.1.9 Ice dynamics considerations

380 As stated in Sect. 1, geodetic mass balance assessments have been often used to calibrate contemporary  
 glaciological measurements. Differences amongst them in relation to vertical surface elevation changes have been  
 attributed to firn densification and ice vertical velocity. Whilst differencing of elevation changes from *dDEM* and  
 glaciological observations should yield representative emergence and submergence velocities (Pelto et al., 2019),  
 385 glaciological data is unfortunately unavailable as part of this study. Alternatively, Belart et al. (2017) implemented  
 a full-Stokes model by ingesting glacier bedrock and surface DEMs, in situ GPS velocities, coupled with the firn  
 densification model derived realistic emergence and submergence velocities. This, however, was beyond the scope  
 of the present study, as the influence of ice dynamics on overall mass budget is usually very small (<5%) on a  
 year-to-year basis and only significant when calculating mass budget over few decades (e.g. Mukherjee et al.  
 390 2022).

### 3.1.10 Uncertainty

395 In spite of the coregistration and bias-correction procedures applied, some of the *dDEM* grids showed systematic  
 residuals on stable terrain [off-glacier] (Table 2). We addressed these biases in elevation change off-glacier  $\sigma_{sys}$   
 as the mean difference between two DEMs (Koblet et al., 2010):

$$\sigma_{sys} = \frac{\sum (H_{DEM_i} - H_{DEM_f})}{n} \quad (5)$$

400 being  $H_{DEM_i}$  and  $H_{DEM_f}$  the elevation of the initial and final DEMs and  $n$  the number of cells on stable terrain.  
 For the calculation of the random uncertainty of the volumetric mass balance estimation  $\sigma_{\Delta v}$ , we considered the  
 volumetric uncertainties on mean elevation change, snow and ice areas and firn densification (see Sect. 4.2), which  
 we summed quadratically to propagate the error:

$$405 \quad \sigma_{\Delta v} = \sum \sqrt{(dh \times \sigma_{A_i})^2 + (A_i \times \sigma_{dh})^2 + (dh_{firn} \times \sigma_{A_i})^2 + (A_i \times \sigma_{dfirn})^2} \quad (6)$$

$\sigma_{A_i}$  being the area uncertainty,  $\sigma_{dh}$  the uncertainty on the rate of elevation change,  $dh_{firn}$  the annual elevation change  
 owed to firn densification, and  $\sigma_{dfirn}$  the uncertainty in firn densification rate. In turn, we calculated  $\sigma_{dh}$  using the  
 410 *patch* method of Berthier et al. (2016), which evaluates the decay of the mean elevation change error on stable  
 terrain (off-glacier) with the averaging area (Wagnon et al., 2021; see also Falaschi et al., 2022). Since we  
 attributed a different density and related uncertainty to the snow and ice area classes (snow:  $\pm 60 \text{ kg m}^{-3}$ ; ice:  $\pm 10$   
 $\text{kg m}^{-3}$ ), we calculated the uncertainty of each class separately, by adding the density uncertainty  $\sigma_{\rho_{\Delta v}}$  of each  
 surface to the volumetric uncertainty in Eq. (5):

$$415 \quad \sigma_m = \sum \sqrt{\frac{(\rho_{\Delta v} \times \sigma_{\Delta v})^2 + (\Delta v \times \sigma_{\rho_{\Delta v}})^2}{\bar{A}}} \times t^{-1} \quad (7)$$

Finally, to obtain the overall glacier-wide mass balance uncertainty  $\sigma_{m,tot}$ , we summed the uncertainties of the  
 snow and ice areas quadratically:

$$420 \quad \sigma_{m,tot} = \sqrt{\sigma_{m,ice}^2 + \sigma_{m,snow}^2} \quad (8)$$

### 3.2 Glacier Index: wet snow and firn area ratios derived from Sentinel-1 and Landsat OLI imagery

425 We implement the Glacier Index of Huang et al. (2022) to characterize glacier accumulation regimes and  
 validate our geodetic results. To account for different glacier areas between the study sites, we express firn and  
 wet snow areas on each region as a fraction of the total glacier area (hereafter referred to as firn area ratio and wet  
 snow area ratio). This ratio can vary to a great extent across different geographic regions through time, whilst



interannual variations of the firn area ratio remain relatively small. The Glacier Index  $I$  is then defined as the difference between the firn and wet snow area ratios

430

$$I = \frac{A_{\text{firn}}}{A_{\text{total}}} - \frac{A_{\text{wet.snow}}}{A_{\text{total}}} \quad (9)$$

where  $A_{\text{firn}}$  is the firn zone area,  $A_{\text{wet.snow}}$  the wet snow zone area and  $A_{\text{total}}$  the total glacier area. The Index is expected to be positive for winter accumulation-type glaciers, as summer snowfall is rare and hence  $A_{\text{wet.snow}} < A_{\text{firn}}$ . In contrast, the Index is more likely to be negative (i.e.  $A_{\text{wet.snow}} > A_{\text{firn}}$ ) for summer-glaciers due to recurring summer solid precipitation. We classified regions and glaciers as winter accumulation-type where  $I \geq 0.05$  and summer-accumulation type where  $I < 0.05$  following Huang et al. (2022).

To discriminate wet snow areas (in late summer) and firn areas (in winter) over glaciers in our selected study areas, we used Landsat OLI and Sentinel-1 imagery on Google Earth Engine (Gorelick et al., 2017). First, the Landsat scenes are used to recognize debris-covered and debris-free areas (ice and snow) on glaciers surface applying a threshold to the previously computed Normalized Difference Snow Index [NDSI] (Bruns et al., 2014). Then, since the Sentinel-1 C-band is sensitive to snow wetness and roughness (Huang et al., 2013), the backscattering properties between the different glacier facies are sufficiently different to discriminate the frozen firn in winter (here defined as the period between January and March) and wet snow zone in late summer (defined here as the time interval from July 20 to September 10) using backscatter coefficients (Fig. 3). For full methodological details we refer to the Supplementary Material in Huang et al. (2022).

### 3.3 Investigating the influence of climate (temperature and precipitation) to govern glacier mass balance

To understand how the precipitation and temperature may have influenced the response of the glaciers in the study sites, we used remotely-sensed daily Global Precipitation Measurement (GPM) IMERG (Hou et al. 2014, Huffman et al. 2015) late run precipitation observations (availability: June 2000 – 2022). The multi-satellite precipitation estimates are obtained using quasi-Lagrangian time interpolation. The algorithm integrates all satellite microwave and infrared precipitation estimates with precipitation gauges and other precipitation estimators for the entire globe and is expected to provide realistic estimates of precipitation. We opted to use the GPM precipitation dataset over either reanalysis data (e.g. ERA5, HARv2), since they have proven to largely over- or underestimate precipitation over the Tibetan Plateau (Wortmann et al., 2018; Lin et al., 2021). Moreover, Huang et al. (2022) have shown how both reanalysis (APHRODITE, ERA5, HARv2) and instrumental records (or instrumental records (e.g. the Taxikorgan climate station) are difficult to link with glacier accumulation regimes in several regions throughout High Mountain Asia. We use temperature estimates from ERA5 Land (Hersbach et al. 2020, Munoz-Sabater et al. 2021) (availability: Jan 1950-July 2022), a gridded reanalysis data based on numerical weather prediction models.

We converted the daily GPM precipitation data to monthly data and calculated the monthly solid precipitation as all the precipitation when the corresponding temperature is less than 0°C. To estimate seasonal temperature and solid precipitation, we assumed May-October as summer months and November-April as winter months. We then obtained the total amount of solid precipitation for each year by matching with the dates/months of the geodetic data as shown in Table S1.

To determine the relation between glacier mass balance and climate variability, we first found the mean annual, winter and summer average (temperature and snowfall) over the 2001-2022 time periods and then calculated annual and seasonal mean temperature and total snowfall anomalies. Finally, we correlated the glacier-wide mass budgets with the annual and seasonal variations of temperature and snowfall. To do this, we used our mass budget estimates at annual scale, added the geodetic mass balance values in Bhattacharya et al. (2021) and performed a correlation analysis using the averaged climate records for analogous sub-periods. Whilst we focus on our shorter 2020-2022 period, our aim was to evaluate climate conditions of the last three years in a longer climate/mass balance context.

## 4 Results

### 4.1 Geodetic mass balance in Muztag Ata and Western Nyainqêntanglha

The glacier-wide, annual geodetic mass balances in Muztag Ata varied from moderately negative to slightly positive conditions (Fig. 4; Table 3).  $B_s$  estimated from Eq. (3) was negative for 2020 (when at its most negative,  $-0.19 \pm 0.14$  m w.e.) and 2022 glaciological years but rather positive in 2021 (Table 3). In terms of seasonal mass balance, the 2022 winter mass budget was positive, whereas the summer budget was negative (Table 3). On an individual glacier basis, both the annual and seasonal mass balances of the (largest and debris-covered) Kekesayi Glacier matched the overall trends of the broader Muztag Ata massif. Interestingly, the annual mass



490

balance estimates of Muztag Ata No. 15 Glacier yielded positive values for all three surveyed years, whilst the seasonal winter (positive) and summer (negative) budgets closely followed the general pattern in Muztag Ata, respectively (Table 3).

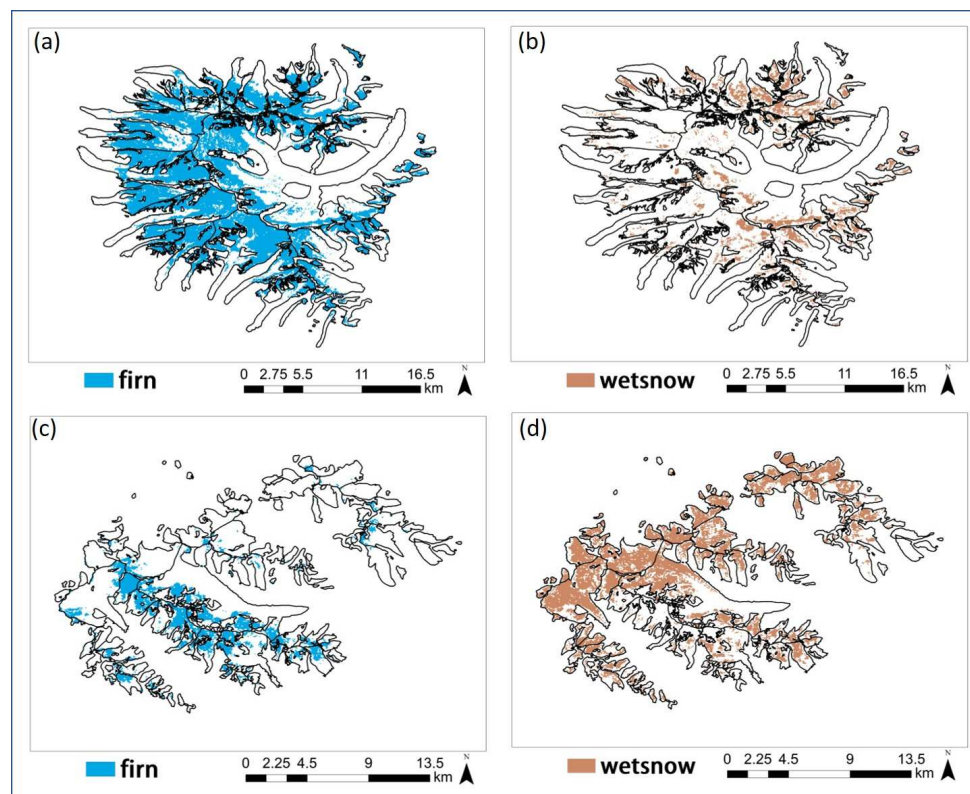
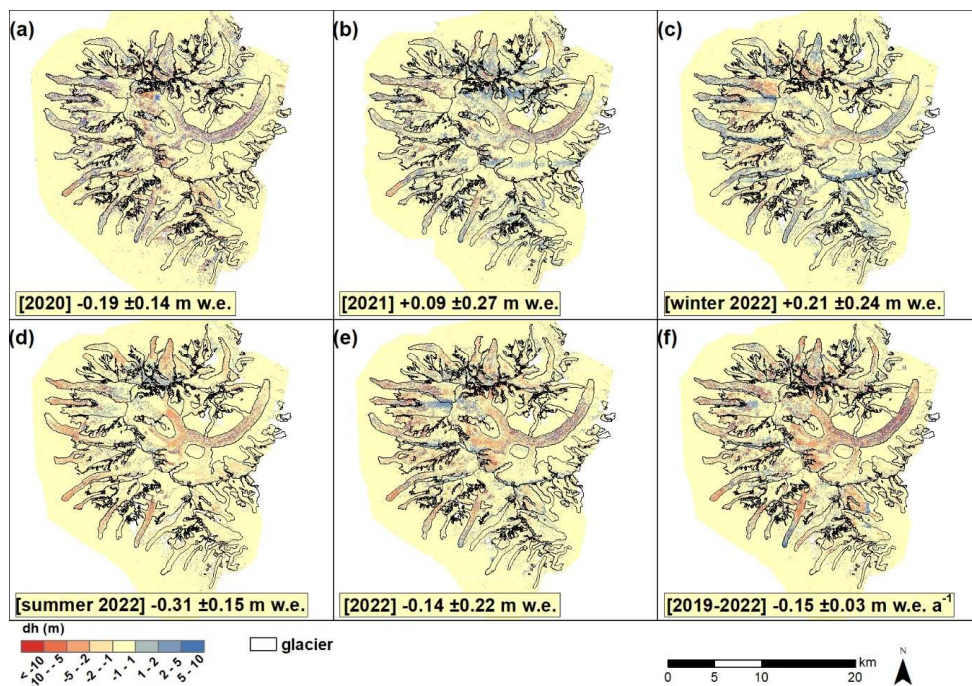


Figure 3. Examples of firn and wet snow cover retrieval in winter and summer 2021 in Muztag Ata (a, b) and Western Nyainqentanglha (c, d).

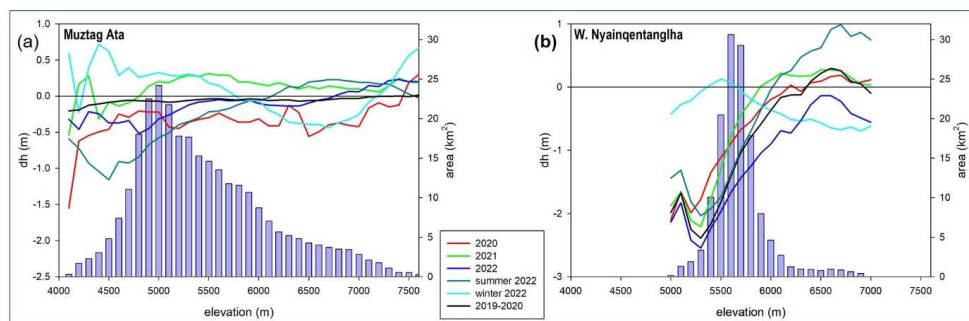
495

The hypsometric distribution of elevation changes in Muztag Ata (Fig. 5a) reveals the lack of a clearly defined elevation change (i.e. mass balance) gradient. Periods with a positive mass budget (2021, winter 2022) show elevation gains at different elevation ranges. They occurred from 4800 m up to the uppermost reaches of the glacierized area (7600 m) during 2021, whereas the winter 2022 shows thickening below 5700 m and above 7200 m and elevation loss in between. Elevation gains (accumulation) during the year 2020 and the summer of 2022 were restricted to elevations >6100 m, whilst in the winter of 2022 elevation gains occurred above 7400 m only. In contrast to Muztag Ata, the annual mass balance of glaciers in Western Nyainqentanglha showed a consistent, highly negative signal, with a negative peak of  $-0.70 \pm 0.22$  in 2022 (Fig. 6; Table 3). While the winter mass budget was balanced, the summer mass budget was strongly negative (Table 3). It must be noted though, that the interannual and seasonal variability in mass balance are not fully comparable due to the incomplete coverage of the study site in the 2021 Pléiades acquisition. The largest, debris-covered Xibu Glacier had also a highly negative mass loss throughout the study period. Contrary to the overall seasonal budgets in Western Nyainqentanglha, Xibu Glacier lost mass during both the summer and winter seasons. Compared to Xibu Glacier, the mass loss of Zhadang Glacier was even greater on the annual scale (peaking at  $-1.12 \pm 0.21$  m w.e. in 2021), but interestingly, recovered during the 2022 winter season (Table 3). In Western Nyainqentanglha, there are clear annual (and 2022 summer) elevation change gradients, in contrast to Muztag Ata. They depict a steep, positive gradient from lower to higher elevations, with elevation gains starting between 5900-6200 m (Fig. 5b). The 2022 annual hypsometric curve, though similar in shape to the two previous years, shows that all of the sampled glacier area underwent ice thinning over this interval. The 2022 winter curve shows slight elevation gains around 5500 m (coinciding with maximum area per elevation band), yet this does not counterbalance all the elevation losses elsewhere in the ice area.

515



520 **Figure 4.** Annual (a, b, e, f) and seasonal (c, d) surface elevation change grids over Muztag Ata and associated geodetic mass balance estimates.



525 **Figure 5.** Hypsometric curve of glacier surface elevation changes over glacierized area in Muztag Ata (a) and Western Nyainqentanglha (b). The light blue bars represent the ice area distribution on 100 m elevation bins for the 2019 glacier area on the right axis.



**Table 3.** Summary of time-interval volume changes ( $10^6 \text{ m}^3$ ) and mass balance (m w.e.) for the total glacier area and selected glaciers. Mass balance values in the 2020-2022 column are provided in m w.e.  $\text{a}^{-1}$ . Values in parenthesis () are calculated using a density of  $850 \text{ kg m}^{-3}$  and values in brackets [] with a 3-year weighted density (see Sect. 6.4.1 for details).

	2020		2021		winter 2022		summer 2022		2022		2020-2022	
	$\Delta v$	$\Delta m$	$\Delta v$	$\Delta m$	$\Delta v$	$\Delta m$	$\Delta v$	$\Delta m$	$\Delta v$	$\Delta m$	$\Delta v$	$\Delta m$
<b>Muztag Ata total glacier area</b>	-90.6 ±36.9	-0.19 ±0.14	+46.7 ±71.1	+0.09 ±0.27	+76.6 ±64.5	+0.21 ±0.24	-106.2 ±78.1	-0.31 ±0.15	-56.3 ±58.0	-0.14 ±0.22	-52.0 ±10.7	[-0.15 ±0.03] (-0.14 ±0.03)
<b>No. 15</b>	0.1 ±0.2	+0.08 ±0.35	0.1 ±0.4	+0.07 ±0.25	+0.6 ±0.4	+0.41 ±0.22	-0.2 ±0.8	-0.13 ±0.20	+0.1 ±0.4	+0.08 ±0.24	+0.2 ±0.1	[+0.09 ±0.04] (+0.08 ±0.04)
<b>Kekesayi</b>	-36.6 ±12.2	-0.31 ±0.17	+18.7 ±23.5	+0.14 ±0.33	+25.5 ±20.9	+0.24 ±0.29	-35.2 ±41.9	-0.44 ±0.30	-22.8 ±19.4	-0.21 ±0.27	-22.9 ±3.6	[-0.29 ±0.04] (-0.26 ±0.04)
<b>Western Nyainqentanglha total glacier area</b>	-103.7 ±16.8	-0.43 ±0.16	-83.5 ±8.9	-0.68 ±0.08	-10.5 ±63.2	-0.04 ±0.27	-152.3 ±13.5	-0.66 ±0.07	-155.8	-0.70 ±0.22	-168.4 ±4.8	[-1.04 ±0.11] (-0.93 ±0.10)
<b>Zhadang</b>	-1.5 ±0.3	-0.80 ±0.41	-1.3 ±0.2	-1.12 ±0.21	+0.3 ±1.0	+0.28 ±0.31	-2.1 ±0.3	-0.83 ±0.12	-1.7 ±0.3	-0.68 ±0.21	-2.1 ±0.1	[-1.61 ±0.16] (-1.44 ±0.15)
<b>Xibu</b>	-17.9 ±3.9	-0.47 ±0.22	-14.7 ±2.3	-0.61 ±0.17	-3.9 ±13.8	-0.16 ±0.35	-20.9 ±3.5	-0.58 ±0.10	-28.4 ±3.6	-0.65 ±0.41	-27.4 ±1.1	[-0.99 ±0.22] (-0.89 ±0.20)

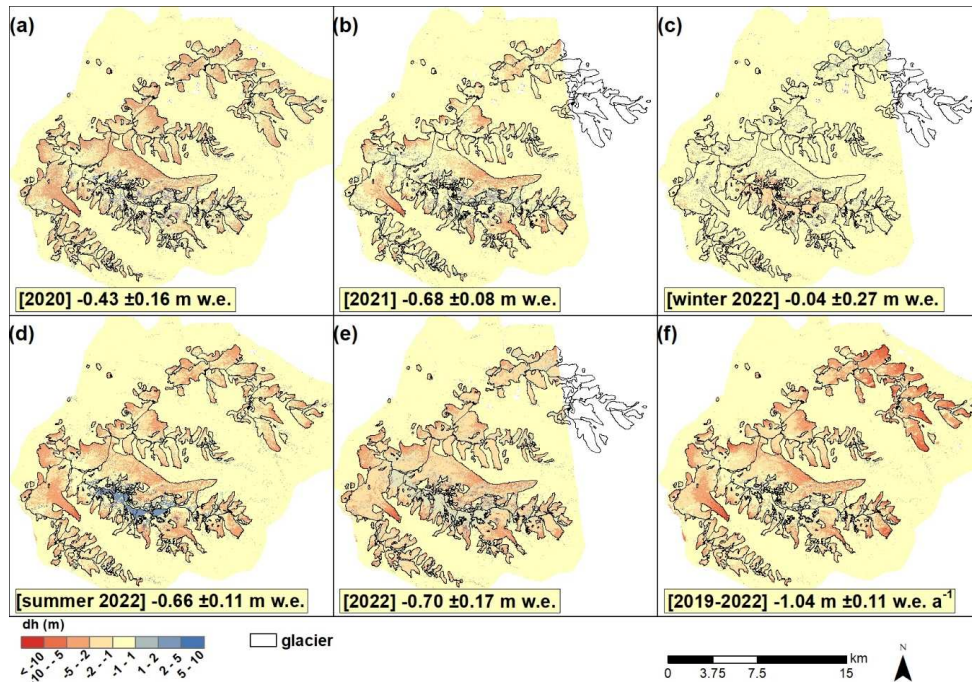


Figure 6. Annual (a, b, e, f) and seasonal (c, d) surface elevation change grids over Western Nyainqentanglha and associated geodetic mass balance estimates.

535

#### 4.2 Wet summer snow and winter firn area ratios derived from the Glacier Index

Firn area and wet snow-ratios varied between 0.55 - 0.6 and 0.15 - 0.23 in Muztag Ata and 0.25 - 0.28 and 0.33 - 0.66 in Western Nyainqentanglha, respectively (Fig. 7 and Table S2). These ratios yielded Glacier Index values between 0.32 and 0.45 in Muztag Ata and -0.38 and -0.07 in Western Nyainqentanglha. To provide a measure of the individual glacier variability, the Glacier Index in Kekesayi and Muztag Ata No. 15 glaciers varied between 0.17 to 0.28 and 0.68 to 0.89, whilst in Xibu and Zhadang glaciers the Index ranged between -0.25 to -0.04 and -0.51 to -0.05, respectively. Based on these assessments, we attribute a winter accumulation regime for Muztag Ata and a summer accumulation regime in Western Nyainqentanglha. Moreover, the evolution of the summer wet snow area ratio points at 2020 as the most negative mass balance year in Western Nyainqentanglha and the year 2019 in Muztag Ata.

540

545

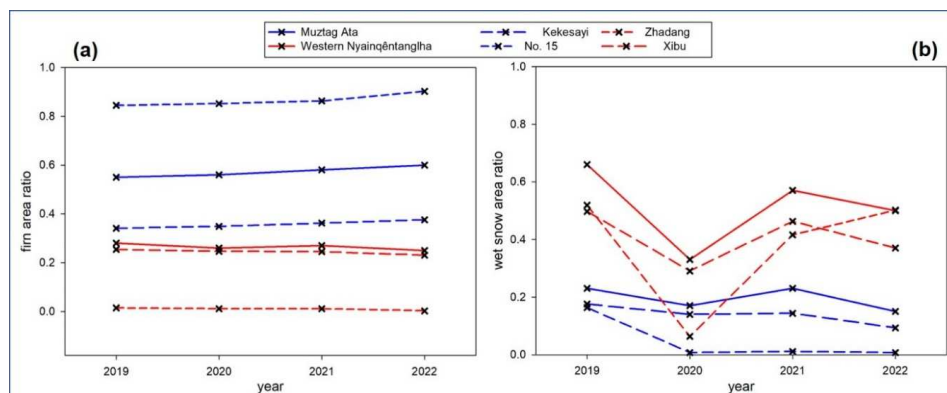


Figure 7. Evolution of the firn area- (a) and wet snow area-ratio (b) between 2019 and 2022.

550

#### 4.3 Relation between climate (temperature and precipitation) and mass balance



In Muztag Ata, the summer (+0.5 °C to -1.1 °C) and winter (-0.9 °C and +0.3 °C) temperature anomalies were either positive or negative among the surveyed 2020 to 2022 years, and showed no prominence within the 2001-2022 period (Fig. 8c,e). In contrast, winter snowfall anomalies were all positive between 2020 and 2022, but still within the 2001-2022 range. It must be also noted that snowfall anomalies (either winter or summer) are of rather small magnitude, especially compared to those in Western Nyainqêntanglha. These results indicate that air temperatures and solid precipitation in the 2020 and 2021 surveyed years were representative of recent climate conditions in Muztag Ata. We were, however, unable to find any significant correlation between climate variability and mass balance in Muztag Ata (Fig. 8a-f). Winter temperatures showed the highest correlation coefficient ( $r = 0.57$ ;  $p = 0.23$ ;  $\alpha = 0.05$ ) amongst the investigated climate variables in Muztag Ata. In Western Nyainqêntanglha, the surveyed 2020-2022 years all had positive summer temperature departures (around +0.6 °C), which were at the same time amongst the highest since in the last two decades (summer departure range: -1.2 °C to +0.7 °C). The 2021 and 2022 winter seasons also showed positive temperature anomalies (+1.6 °C and +0.6 °C; winter departure range: -3.3 °C to +3.0 °C; Fig. 8g-j). Of the last 16 years, summer air temperatures have experienced positive anomalies. Likewise, the winter season has also shown positive temperature anomalies for 8 of the last 10 years. The years 2021 and 2022 were thus among the warmest and driest in Western Nyainqêntanglha in the last two decades approximately. We found a rather strong (though not significant at the 95% confidence interval) correlation between temperature anomalies and mass balance at both annual ( $r = 0.78$ ,  $p = 0.08$ ) and seasonal ( $r = 0.56$ ,  $p = 0.25$  and  $r = 0.69$ ,  $p = 0.12$  for summer and winter, respectively) scale. In regard to solid precipitation, our surveyed years showed highly negative summer anomalies (up to ~16 mm/year). This likely had an impact on the overall negative annual snowfall anomalies, which in turn have been negative since 2014. Overall, the correlation between mass balance and solid precipitation was weak ( $r < 0.39$ ) and non-significative either at annual or seasonal scale.

575

## 5. Discussion

### 5.1 Methodological constraints

#### 580 5.1.1 Internal consistency of the geodetic mass balance estimates

To verify the consistency of our high-resolution geodetic mass balance surveys at annual to seasonal mass balance, we tested the internal robustness of our geodetic surveys. We evaluated the residuals between accumulated vs. the sum of individual survey periods encompassing identical time intervals, in so-called 'triangulation' tests. This is a way to measure the impact of using different inputs (*dDEM* grids, snow and ice distribution maps, and the resulting average material density) on geodetic mass balance values when evaluating similar periods yet at different time steps.

On a glacier-wide scale, the difference between the sum of the Muztag Ata 2022 summer and winter mass balances (-0.10 m w.e.), and accumulated 2022 annual budget (-0.14 ± 0.22 m w.e.) yielded a difference of ± 0.04 m w.e. between both measurements. In the case of Western Nyainqêntanglha, this glacier-wide comparison showed no differences between the accumulated and added values (both -0.70 m w.e.). In addition, and on an individual glacier scale, we found a minimal discrepancy of ± 0.01 m w.e. for Kekesayi Glacier, whilst a much larger difference was found for the Muztag Ata No. 15 (± 0.28 m w.e.) mass budgets. Individually, Zhadang and Xibu glaciers in Western Nyainqêntanglha showed differences between 0.09-0.13 m w.e.a<sup>-1</sup>.

Overall, we find the glacier-wide and (for the most part) individual differences to be well within the uncertainty ranges, and attribute the differences to the overall small differences in average density (which in turn derives from the snow and ice distribution) of the September 2021 (590 kg m<sup>-3</sup>) and April 2022 Sentinel-2 (630 kg m<sup>-3</sup>) snow and ice masks. In this sense, Pelto et al. (2019) showed how the spatial distribution of material densities has a larger impact on seasonal mass balances compared to the assumed density values themselves. In contrast, variable density distribution has a greater impact when smaller areas are considered, e.g. in the case of Muztag Ata No. 15.

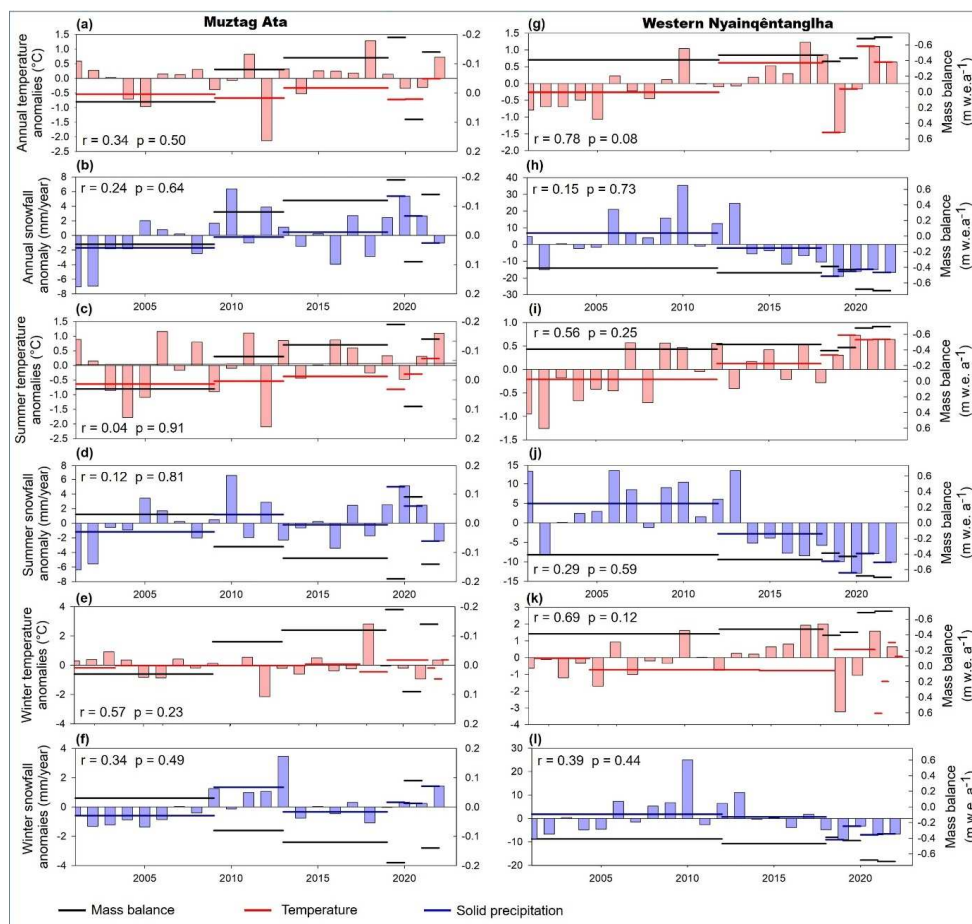
A second consistency test was carried out to test the impact of varying density assumptions in more detail, evaluating the accumulated 2020-2022 mass budget and the sum of all the individual annual periods. We calculated these differences using a single *dDEM* grid and a) an overall density of 850 ± 60 kg m<sup>-3</sup> and b) a 3-year weighted density (Muztag Ata = 774 ± 60 kg m<sup>-3</sup>; Western Nyainqêntanglha = 762 ± 60 kg m<sup>-3</sup>) for all the mass involved following Huss (2013) (Table 3). In Muztag Ata, the 2020-2022 glacier-wide estimate (-0.14 ± 0.03 m w.e. a<sup>-1</sup> [scenario a] and -0.14 ± 0.03 m w.e. a<sup>-1</sup> [scenario b]) was similar to the averaged mass budget of the individual periods (-0.08 ± 0.21 m w.e. a<sup>-1</sup>). The accumulated 2020-2022 mass balance of Kekesayi (-0.29 ± 0.04 m w.e. a<sup>-1</sup> [a]; (-0.26 ± 0.04 m w.e. a<sup>-1</sup> [b]) differed in ± 0.16 and ± 0.13 m w.e. a<sup>-1</sup>, respectively, from the averaged individual periods (-0.13 ± 0.26 m w.e. a<sup>-1</sup>). Differences were negligible in the case of Muztag Ata No. 15 Glacier.

610



615

In Western Nyainqêntanglha, the differences were much larger ( $-0.60 \pm 0.15$  m w.e.  $a^{-1}$  on average vs.  $-1.04 \pm 0.11$  m w.e.  $a^{-1}$  [scenario a] and  $-0.93 \pm 0.10$  m w.e.  $a^{-1}$  [scenario b]). Expectedly, even larger differences were found for Zhadang and Xibu glaciers, since higher thinning rates will have a greater impact on any given density value. The use of 3-year weighted densities of Huss (2013) tends to reduce the differences between the accumulated vs. added mass budgets, confirming that constant density values should be kept only for time spans  $>3$  years, whereas a more thorough density inspection is preferable for shorter timescales (Belart et al., 2017; Klug et al., 2018).



620

**Figure 8.** Evolution of geodetic glacier mass balance compared to annual and seasonal temperature and snowfall anomalies in Muztag Ata (a-f) and Western Nyainqêntanglha (g-l). In the temperature panels, the mass-balance values on the right axis have been reversed for a better interpretation.

### 5.1.2 Potential and limitations of Pléiades DEMs for assessment of short-term geodetic mass balance

625

Among the various uncertainty sources introduced in geodetic mass balance assessments at high temporal and spatial resolution, the ability to consistently map glacier surfaces, the density assumptions and especially DEM precision and overall quality have probably the highest impact on the final uncertainty estimate (Beraud et al., 2022). Here we discuss the suitability of our Pléiades DEM dataset to quantify both annual and seasonal mass balances over areas with contrasting glacier mass change rates.

630

Because 90% of the annual (seasonal) glacier elevation changes in Muztag Ata and Western Nyainqêntanglha range between  $-4.7$  m to  $+3.3$  m, highly accurate and precise DEMs are needed to account for the resultant small magnitude of glacier mass fluctuations. In Sect. 3.1.4 we reported that our DEMs errors are within previously reported biases of Pléiades DEMs used in geodetic mass balance assessments (e.g. Berthier et al., 2014; Denzinger et al., 2021; Falaschi et al., 2022). A fine coregistration between DEMs allows the minimization of vertical and





635 horizontal biases. This is especially important when utilizing DEMs acquired when seasonal snow is present off-  
glacier, but difficult to circumvent when surveying mass balance during accumulation periods. Under these  
conditions, vertical shifts ~1 m measured over stable terrain have been reported (Beraud et al., 2022). Glaciers  
close to balanced conditions (such as Muztag Ata) are particularly sensitive to an adequate quantification of  
systematic biases compared to glaciers with a much more negative mass budget, as a given small vertical DEM  
640 adjustment may shift from slightly negative to slightly positive elevation changes and vice-versa.  
Around our reported biases, the vertical precision (standard deviation on stable terrain) of our Pleiades time series  
in Muztag Ata and Western Nyainqêntanglha Pleiades were  $\pm 2.1$  m and  $\pm 1.2$  m on average, respectively (Table  
2). DEM precision can be also described using the normalized median absolute deviation (NMAD), which is  
less sensitive to outliers compared to standard deviation (Dehecq et al., 2016). Independently from seasonal snow  
645 conditions, the NMAD over off-glacier terrain was consistently around  $\pm 1.3$  m in Muztag Ata, and varied between  
 $\pm 0.6$  m and 1.2 m in Western Nyainqêntanglha. These standard deviations and NMAD values are in the same  
order of magnitude as other very high resolution DEMs used in glaciological applications (Berthier et al., 2014;  
Belart et al., 2017; Pelto et al., 2019; Beraud et al., 2022). Comparatively, the lower precision in the Muztag Ata  
DEMs result in relatively larger uncertainties in particular cases (Table 3). This becomes more problematic due  
650 to the short temporal baseline, and when glaciers are close to in-balance conditions. With these caveats in mind,  
our annual and seasonal geodetic mass balance estimates were robust and consistent with the results retrieved  
from the Glacier Index (see Sect. 5.2) and hence can provide valuable insight into glacier accumulation regimes  
in High Mountain Asia.

## 655 5.2 Discerning accumulation regimes

The heterogeneity of regional climates displayed in High Mountain Asia, from monsoon-dominated regions with  
abundant precipitation occurring in the warm season to areas where westerly-induced, winter precipitation  
prevails, results in diverse glacier behaviour and sensitivity to climate drivers (Bolch et al., 2012; Sakai and Fujita,  
660 2017). This, added to the sparsity of glaciological in situ observations, poses a fundamental challenge for  
understanding the response of the region's glaciers to climatic change. More so, the inadequate number of  
meteorological stations placed at glacier altitude often means that only distant, lower elevation instrumental  
records are available for glacier studies of local extent. Climatic conditions at low-lying valleys, however, can  
deviate substantially or even be entirely unrepresentative of those met by glaciers at high elevation (Wortmann  
665 et al., 2018). Consequently, a major gap for a better understanding of glacier mass changes in response to climatic  
change and their frozen water storage lies in the sparse knowledge of climate conditions at glacier elevations in  
general, precipitation and snow accumulation in particular (Miles et al., 2021; Vishwakarma et al., 2022).  
Huang et al. (2022) showed important discrepancies in accumulation regimes for some regions across High  
Mountain Asia between 2015 and 2018, as derived from gridded climate datasets (including APHRODITE, ERA5  
670 and HARv2 products) on the one hand, and the SAR-derived Glacier Index on the other hand. In the specific case  
of the Muztagh Ata area, there is conflicting evidence about whether glaciers are of winter- or summer-  
accumulation type. Data from the nearest Taxikorgan station indicate that precipitation occurs mainly during  
summer time [April-September] (Zhu et al., 2018a), so that a summer accumulation regime may be assumed for  
the Muztag Ata glaciers. Indeed, Zhu et al. (2018a, b) pointed out as summer precipitation as the main driver of  
675 the Muztag Ata No. 15 Glacier mass balance, and that higher amounts of solid precipitation in summer compared  
to the cold season were mostly responsible for the overall positive budget between 1998 and 2012. However, these  
authors also showed that between 1980 and 1997, and in spite of heavier precipitation in summer compared to  
winter, other processes affecting glacier mass balance (e.g. snowmelt, sublimation) resulted in a more negative  
budget in the summer season.  
680 In contrast to the Taxikorgan instrumental records in Muztag Ata, which show higher amounts of precipitation  
during the summer months, Maussion et al. (2014) used HAR data and found that overall, the Pamir region  
experiences mostly winter precipitation. Huang et al. (2022) found a conspicuous mismatch between the  
(transitional) accumulation regime derived from a) gridded climate datasets and climate stations off-glacier and  
b) the winter accumulation-type according to the SAR analyses. The authors noted the substantial differences in  
685 snow accumulation measured at ~7000 asl (605 mm a<sup>-1</sup>) and those recorded at Taxikorgan station between 1960  
and 2002 [60-70 mm; Duan et al. (2015)], suggesting that the upper part of Muztag Ata [(an anomalously high  
peak in the region, Seong et al., 2009)] may be affected by a different atmospheric circulation system compared  
to the valley bottoms (i.e. at Taxikorgan station elevation). Sakai et al. (2015) used a summer- to annual-  
precipitation ratio from APHRODITE data and Temperature-Precipitation plots as indicators of glacier sensitivity  
690 to climate changes and put the glaciers in Eastern Pamir within the winter accumulation (and less sensitive)  
envelope. Although our Pleiades datasets have allowed us to retrieve mass changes for two seasonal intervals  
only, the geodetic estimates of the glacier-wide Muztag Ata 2022 winter ( $+0.21 \pm 0.24$  m w.e.) and summer ( $-0.31$   
 $\pm 0.15$  m w.e.) mass balance favor a winter accumulation-type scenario for the Muztag Ata glaciers.



695 In stark contrast to Muztag Ata and Eastern Pamir, the summer Monsoon-dominated glaciers in Western  
Nyainqêntanglha have a low annual temperature range, are highly sensitive to temperature and precipitation  
changes, and are therefore prone to strong mass losses (Sakai et al., 2015). There is good consensus in  
characterizing most glaciers in the area as summer accumulation-type (Fujita and Ageta, 2000; Maussion et al.,  
2014; Sakai et al., 2015; Huang et al., 2022). The mass balance of Zhadang Glacier was found to be particularly  
700 sensitive to the onset of the Monsoon period (Kang et al., 2009; Mölg et al., 2012), though mid-latitude westerlies  
too drive its mass balance (Mölg et al., 2014). Our geodetic results for the Western Nyainqêntanglha glaciers  
showed high ablation rates prevailing over accumulation in the 2022 summer season ( $-0.66 \pm 0.07$  m w.e.a<sup>-1</sup>) and  
little mass recovery during the winter season ( $-0.04 \pm 0.27$  m w.e.a<sup>-1</sup>). The 2009-2011 and 2008-2013 mass balance  
of Zhadang Glacier modelled by Zhang et al. (2013) and Zhu et al. (2018a) support our findings, indicating high  
705 mass loss during the ablation (summer) season, but minor losses during the cold (winter) season.

### 5.2.1 Insight from climate records and the Glacier Index

710 Establishing a clear link between the investigated climate datasets and variables proved to be a challenging task.  
Several of the stronger correlations between glacier mass balance and temperature and solid precipitation were  
not significant, which is most probably due to the small number of mass balance observations ( $n_{\max} = 7$  in the  
1967-2022 correlation tests). In Muztag Ata, our results showed a stronger correlation between glacier mass  
budget and solid precipitation compared to air temperature (though we stress here that neither correlations were  
715 significant). Consequently, snowfall appears to be a stronger mass balance driver in relation to air temperature.  
This is a relevant development, as mass balance in colder and drier environments are influenced by solid  
precipitation to a greater extent (Zhu et al. 2018a, b).

We observed a different scenario in Western Nyainqêntanglha. Correlations were much stronger (and significant)  
between mass balance and temperature anomalies in comparison to solid precipitation. This is not surprising, since  
summer temperatures have a greater impact on glacier mass balance in more humid climatic regions such as  
720 Western Nyainqêntanglha (Zhang et al., 2013, Bhattacharya et al., 2021). Mölg et al., (2014) showed how summer  
precipitation determines the annual mass balance of summer accumulation glaciers in the area. Summer  
temperature, however, modulates the solid/liquid precipitation ratio during the summer season, when most of the  
solid precipitation occurs in the region.

725 The intricacies and limitations of determining accumulation regimes over our investigated glaciers based on the  
available climate records reveal the need for additional complementary approaches. To support our geodetic and  
climate data findings, we implemented the Glacier Index, which bypasses the need for climate data altogether.

The wet snow area- and firn area-ratio showed different patterns and trends in Muztag Ata compared to Western  
Nyainqêntanglha during the 2019-2022 period (Figure 7). In Western Nyainqêntanglha, the annual wet snow area  
are higher than the firn area-ratios, meaning that there is more accumulation in summer than in winter. The  
730 opposite was found in Muztag Ata, where the firn area-ratios are higher than the late summer wet snow area ratio.  
This is in turn indicative of higher accumulation during winter in Muztag Ata. In addition, the firn area-ratio is  
much lower in Western Nyainqêntanglha compared to Muztag Ata, and it is therefore not surprising that glacier  
mass balance has been much more negative for at least the last six decades (Bhattacharya et al., 2021 and  
references therein, see Table 4). These results agree well with our geodetic mass balance results for the annual  
735 and seasonal intervals in the 2020-2022 sampled period (Table 3), which support winter and summer  
accumulation-type regimes in Muztag Ata and Western Nyainqêntanglha, respectively.

Despite the overall good agreement between the proposed accumulation regime types based on both the geodetic  
and Glacier Index approaches, we report a minor caveat. The wet snow area-ratio in Western Nyainqêntanglha  
indicates that the year 2020 should be the most negative mass balance year in the study period ( $-0.43 \pm 0.16$  m  
740 w.e.a<sup>-1</sup> as per our geodetic estimate), whereas the geodetic results suggest 2022 ( $-0.70 \pm 0.22$  m w.e.) as the most  
negative year. A possible explanation lies in the differences in the acquisition dates between the Pléiades and  
Sentinel-1 satellite images used in the geodetic and Glacier Index approaches. The Glacier Index utilizes SAR  
imagery acquired from July 20 to September 10 each year to guarantee wet snow conditions over accumulation  
areas (whereas in late September and October, snow may be dry for areas above 5,000 m asl due to low  
745 temperatures). On the contrary, the 2020 Pléiades scenes employed in the geodetic method were acquired on 8  
October. Our climate data, however, shows that in Western Nyainqêntanglha, more snow fell during September  
2020 compared to August in 2020, which will lead to a lower wet snow area-ratio.

### 5.3 Mass balance differences between both study sites and in the long-term perspective

750 Our mass balance estimates between 2020 and 2022 for the Muztag Ata massif suggest a greater variability in  
mass budget than previously acknowledged in the region (Fig. 9a). During the past six decades, Bhattacharya et  
al. (2021) found mass balance rates between  $+0.03 \pm 0.10$  m w.e. a<sup>-1</sup> and  $-0.14 \pm 0.10$  m w.e. a<sup>-1</sup>. On annual time

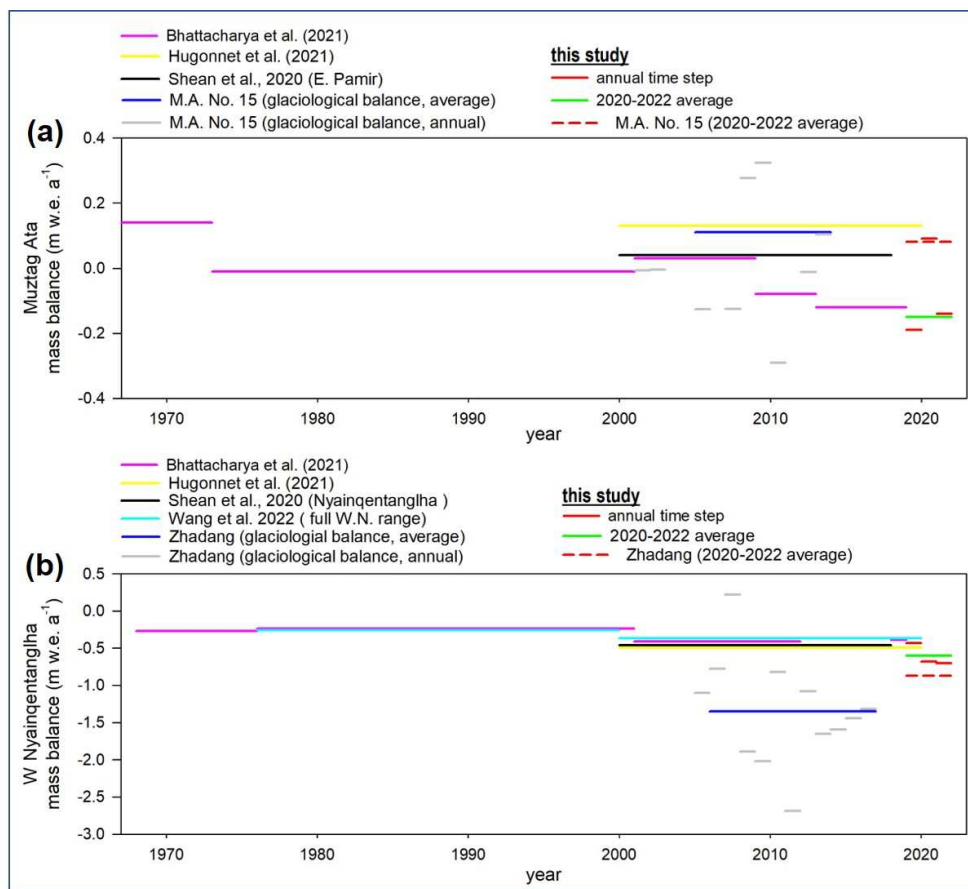


755 steps, our values ranged between  $+0.09 \pm 0.27$  m w.e.  $a^{-1}$  and  $-0.19 \pm 0.14$  m w.e.  $a^{-1}$ , suggesting a greater variability (Table 3). Averaged between 2020 and 2022, the glacier-wide mass balance of Muztag Ata ( $-0.08 \pm 0.20$  m w.e.  $a^{-1}$ ) is similar to the 2013-2019 mean [ $-0.12 \pm 0.09$  m w.e.  $a^{-1}$ ; Bhattacharya et al. (2021)]. This suggests an ongoing trend of slight mass loss in the Muztagh Ata massif for the last three years, meaning a continuation of the very slight mass loss rate observed for most of approximately the last decade (Bhattacharya et al., 2021). A number of studies (Holzer et al., 2015; Lv et al., 2020) report slight, but insignificant positive values between 1999 and 760 2015/2016, whilst Bhattacharya et al. (2021) found in-balance conditions since 1973.

On an individual glacier basis, glaciological measurements exist for the small ( $\sim 1.1$  km<sup>2</sup>) Muztag Ata No. 15 glacier (Fig. 1) between the years 2002 and 2014 (Yao et al., 2012 and unpublished data; Holzer et al., 2015). The mean 2005-2014 mass balance of this glacier was  $+0.11$  m w.e.  $a^{-1}$ , which is similar to our  $+0.08 \pm 0.20$  m w.e.  $a^{-1}$  2020-2022 average.

765 In contrast to Muztag Ata, glaciers in the Western Nyainqêntanglha range show much higher mass loss rates. The 2022 mass balance of  $-0.70 \pm 0.22$  m w.e. is not only much more negative than the  $-0.08 \pm 0.20$  w.e.  $a^{-1}$  2020-2022 average found in Muztag Ata, but also represents a negative maximum for the Western Nyainqêntanglha area itself since the late 1960's (Fig. 9b). Indeed, the mass budget has not been more negative than  $-0.65 \pm 0.08$  m w.e.  $a^{-1}$  approximately the last five decades (Hugonnet et al., 2021 and other sources; Table 4). It must be noted, 770 however, that the sampled glaciers vary among these studies, and the mass budget could have differed if data from different temporal scales were considered.

Zhadang Glacier, which had a glaciological mass balance program running between 2006 and 2017 (Yao T, pers. com.), was one of the glaciers with the most negative mass budget in the Western Nyainqêntanglha range. The 2020-2022 mean mass balance was  $-0.87 \pm 0.28$  m w.e.  $a^{-1}$ , depicting a high mass loss rate consistent with previous 775 modelled ( $-1.0$  m w.e.  $a^{-1}$  [2001-2011], Huintjes et al., 2015;  $-0.91$  w.e.  $a^{-1}$  [2010-2012] approx.; Zhu et al., 2015) and in situ ( $-1.2$  m w.e.  $a^{-1}$  to  $-1.6$  m w.e.  $a^{-1}$  [2009-2014] estimates; Zhang et al., 2013 and 2016). Surprisingly, though, remote sensing-based estimates have yielded significantly less negative mass balances encompassing longer but overlapping periods ( $-0.50 \pm 0.17$  m w.e.  $a^{-1}$  [2000-2014], Li and Lin. (2017);  $-0.60 \pm 0.19$  m w.e.  $a^{-1}$  [2000-2017], Ren et al., (2020)). The average, 2006-2017 in situ mass balance of Zhadang Glacier ( $-1.35$  m w.e.  $a^{-1}$ ; Yao et al., 2012 and unpublished data) was found to be closer to our estimate, which may suggest that 780 penetration correction for mass balance estimates based on DEMs originating from SAR data are inadequate in the area.



785 **Figure 9.** Comparison of geodetic glacier mass balance for the glacier-wide area and specific glaciers with available glaciological mass balance records in Muztag Ata (a) and Western Nyainqentanglha (b).



**Table 4.** Mass balance estimates in Muztag Ata and Western Nyainqêntanglha based on optical and SAR-derived DEM differencing.

	Time period	Mass balance (m w.e.a <sup>-1</sup> )	source
<b>Muztag Ata</b>			
	1967-1973	-0.14 ±0.10	Bhattacharya et al. (2021)
	1973-2001	-0.01 ±0.06	
	2001-2009	+0.03 ±0.10	
	2009-2013	-0.08 ±0.12	
	2013-2019	-0.12 ±0.09	
	1967-2019	-0.06 ±0.07	Holzer et al. (2015)
	1973-1999	-0.04 ±0.42	
	1999-2009	+0.04 ± 0.45	
	2009-2013	-0.07 ±0.53	
	1973-2009	-0.03 ±0.33	Hugonnet et al. (2021)
	2000-2004	+0.19 ±0.08	
	2005-2009	+0.13 ±0.06	
	2010-2014	+0.09 ±0.07	
	2014-2019	+0.07 ±0.08	
	2000-2019	+0.13 ±0.10	Lv et al. (2020)
	2000-2015/2016	+0.16 ±0.03	
	2000-2018	+0.21 ±0.06	Shean et al. (2020)
<b>W. Nyainqêntanglha</b>			
	1968-1976	-0.27 ±0.11	Bhattacharya et al. (2021)
	1976-2001	-0.24 ±0.13	
	2001-2012	-0.41 ±0.11	
	2012-2018	-0.47 ±0.15	
	2018-2019	-0.39 ±0.18	
	1968-2019	-0.32 ±0.09	Hugonnet et al. (2021)
	2000-2004	-0.31 ±0.08	
	2005-2009	-0.44 ±0.06	
	2010-2014	-0.58 ±0.07	
	2014-2019	-0.65 ±0.08	
	2000-2019	-0.49 ±0.17	Shean et al. (2020)
	2000-2018	-0.51 ±0.11	
(total W. Nyainqêntanglha)	2000-2020	-0.37 ±0.12	Wang et al. (2022)
(total W. Nyainqêntanglha)	2000-2017	-0.30 ±0.19	Ren et al. (2020)
(total W. Nyainqêntanglha)	1975-2000	-0.25 ±0.15	Zhou et al. (2018)
(total W. Nyainqêntanglha)	2000-2013/2014	-0.23 ±0.13	Li and Lin (2017)
(total W. Nyainqêntanglha)	2000-2013/2014	-0.30 ±0.07	Zhang and Zhang (2017)

790

### Conclusions

795 In this study we have assessed the capability of very high-resolution Pleiades DEMs to quantify glacier mass balance over short (annual to seasonal) time steps over regions in High Mountain Asia that have shown contrasting mass balance trends in the last few decades. We find intrinsic DEM quality to be the main source of uncertainty in geodetic mass balance estimates, rather than varying seasonal snow conditions among the two study sites. Indeed, the mean vertical precision (NMAD) of Muztag Ata and Western Nyainqêntanglha DEMs were ±1.3 m and ±0.6 m to ±1.2 m, respectively. This, in turn, is along the lines of previously reported values of other very-  
 800 high resolution DEMs used in similar geodetic mass balance estimations worldwide.

Two main conclusions can be drawn from the internal consistency tests (utilized to evaluate the differences between accumulated vs. the sum of individual periods). On one side, the tests confirm that the usage of a semi-automated approach (such as ASMAg) for the identification of different glacier surfaces (ice, snow/firn) (and thus the distribution of assumed material densities) is a robust approach when quantifying glacier mass balance at a multi-glacier scale. Greater differences on individual glaciers, however, suggest that manual mapping by visual interpretation might be preferable, especially on small glaciers. Concurrently, the tests reaffirm that using time-weighted densities reduced the residuals between accumulated vs. added mass budgets, stressing the necessity of  
 805 implementing detailed density distributions over constant values for intervals longer than 3 years.



810 Mean annual ( $-0.11 \pm 0.21$  m w.e.  $a^{-1}$ ) mass balance estimates in Muztagh Ata between 2020 and 2022 point at the  
continuation of the slight mass loss trend after a period of apparently balanced conditions. On the contrary, the  
glacier mass balance in Western Nyainqêntanglha reached a negative peak of  $-0.70 \pm 0.22$  m w.e.  $a^{-1}$  in 2022, which  
represents a new maximum over the last six decades. The analysis of ERA5-land 1950-2021 temperature and  
815 GPM 2001-2021 solid precipitation anomalies confirm that the years 2020 and 2021 as a) average years in terms  
of air temperature and snowfall in Muztagh Ata and b) particularly warm and dry years in Western  
Nyainqêntanglha.  
The 2022 winter and summer mass balance estimates ( $+0.21 \pm 0.24$  m w.e. and  $-0.31 \pm 0.15$  m w.e., respectively)  
in Muztagh Ata suggest a winter accumulation type, whilst mass losses of  $-0.04 \pm 0.27$  m w.e and  $-0.66 \pm 0.07$  m  
w.e. in the winter and summer seasons, respectively, confirm a summer accumulation-type regime in Western  
820 Nyainqêntanglha, with ablation prevailing over accumulation in the summer (ablation) season. With the SAR-  
based Glacier Index, we indirectly validated our geodetic mass balance estimates and the derived inferences that  
were made in relation to glacier accumulation types in Muztagh Ata and Western Nyainqêntanglha. Whilst the  
Index does not provide a specific mass balance estimate per se that can be directly compared against geodetic (or  
glaciological) results, it can provide further insight into accumulation regimes in poorly known regions. Moreover,  
825 it fully bypasses the need for instrumental or reanalysis records, which are often unavailable or unrepresentative  
of climate conditions at glacier locations. Further geodetic and glaciological mass balance measurements in  
combination with such an Index will open new possibilities in glaciological research.  
Based on the above, we conclude that our DEM time series and mass budget estimates proved to be consistent for  
making reliable, short-term estimations of glacier mass balance using a remote sensing-based approach. The ever-  
830 increasing number and availability of very-high resolution optical satellites (with stereo capability and relatively  
short revisit time) will allow for increasing the number of glaciers in isolated regions that can be readily  
monitored.

#### Code availability

835 We are grateful to Etienne Berthier for kindly providing the along-track bias correction and the elevation change  
uncertainty “patch” tools.  
The DEM generation code from Shean et al. (2016) is available from the corresponding github repository at  
<https://github.com/NeoGeographyToolkit/StereoPipeline>. The DEM coregistration code (Nuth and Kääb, 2011)  
840 is available at <https://github.com/GeoUtils/geoutils>.

#### Data availability

845 The Sentinel-2 scenes were obtained from the USGS EarthExplorer data poll (<https://earthexplorer.usgs.gov/>) and  
the ESA Copernicus Open Access Hub (<https://scihub.copernicus.eu/>). The Sentinel-1 and Landsat OLI scenes  
used in the Glacier Index are available online on Google Earth Engine through the Google Cloud Storage and the  
Google Cloud public data program. The elevation change grids from Bhattacharya et al. (2021) are available from  
PANGAEA at <https://www.pangaea.de> and <https://www.mountcryo.org/datasets/>. The elevation change maps  
from Hugonnet et al., 2021 are publicly available at <https://doi.org/10.6096/13>. The ERA5-Land data was  
850 downloaded from the Copernicus Climate Data Store at <https://cds.climate.copernicus.eu/>.

#### Author contribution

855 DF and TB designed the study. OK contributed to the study design. DF led the study, processed and analyzed data  
and wrote the manuscript. AB, KM and LH, PR processed and analyzed data. AB, KM, LH, OK and TB  
contributed to the writing of the manuscript. TB and TY secured the funding. The order of authors from third to  
seventh is in alphabetical order.

#### Competing interests

860 Some authors are members of the editorial board of The Cryosphere. The peer-review process was guided by an  
independent editor, and the authors have also no other competing interests to declare.

#### Acknowledgements

865 We are grateful to CNES/Airbus DS for the provision of the Pléiades satellite data within the ISIS program for  
reduced costs. Pleiades © CNES 2020/2021/2022 and AIRBUS DS. We would like to thank Christine Baron,  
Sylvie Boureausseau, and the whole Airbus Intelligence Team for their assistance during the acquisition of the



870 Pléiades imagery. AB acknowledges funding by the Science & Engineering Research Board (SERB), Department of Science & Technology (DST), India (grant no. CRG/2021/002450).

#### Funding

875 This study was supported by the Strategic Priority Research Program of Chinese Academy of Sciences (XDA20100300) and the Swiss National Science Foundation (200021E\_177652/1) within the framework of the DFG Research Unit GlobalCDA (FOR2630) and benefited from the research cooperation within the Dragon 5 program supported by ESA and NRSCC (4000136930/22/I-NB).

#### 880 References

- Abdel Jaber, W., Rott, H., Floricioiu, D., Wuite, J., and Miranda, N.: Heterogeneous spatial and temporal pattern of surface elevation change and mass balance of the Patagonian ice fields between 2000 and 2016, *Cryosphere*, 13(9), 2511–2535, <https://doi.org/10.5194/tc-13-2511-2019>, 2019.
- 885 Andreassen, L. M., Elvehøy, H., Kjöllmoen, B., and Engeset, R. V.: Reanalysis of long-term series of glaciological and geodetic mass balance for 10 Norwegian glaciers, *Cryosphere*, 10(2), 535–552, <https://doi.org/10.5194/tc-10-535-2016>, 2016.
- Armstrong, W. H., Polashenski, D., Truffer, M., Horne, G., Hanson, J. B., Hawley, R. L., Hengst, A. M., Vowels, L., Menounos, B., and Wychen, W. V.: Declining basal motion dominates the long-term slowing of Athabasca Glacier, Canada, *J. Geophys. Res. Earth. Surf.*, 127(10), <https://doi.org/10.1029/2021JF006439>, 2022.
- 890 Belart, J. M. C., Berthier, E., Magnússon, E., Anderson, L. S., Pálsson, F., Thorsteinsson, T., Howat, I. M., Aðalgeirsdóttir, G., Jóhannesson, T., and Jarosch, A. H.: Winter mass balance of Drangajökull ice cap (NW Iceland) derived from satellite sub-meter stereo images, *Cryosphere*, 11(3), 1501–1517, <https://doi.org/10.5194/tc-11-1501-2017>, 2017.
- 895 Belart, J. M. C., Magnússon, E., Berthier, E., Pálsson, F., Aðalgeirsdóttir, Gu., and Jóhannesson, T.: The geodetic mass balance of Eyjafjallajökull ice cap for 1945–2014: Processing guidelines and relation to climate, *J. Glaciol.* 65(251), 395–409, <https://doi.org/10.1017/jog.2019.16>, 2019.
- Beraud, L., Cusicanqui, D., Rabatel, A., Brun, F., Vincent, C., and Six, D.: Glacier-wide seasonal and annual geodetic mass balances from Pléiades stereo images: Application to the Glacier d’Argentière, French Alps, *J. Glaciol.*, 1–13, <https://doi.org/10.1017/jog.2022.79>, 2022.
- 900 Berthier, E., and Brun, F.: Karakoram geodetic glacier mass balances between 2008 and 2016: Persistence of the anomaly and influence of a large rock avalanche on Siachen Glacier, *J. Glaciol.*, 65(251), 494–507, <https://doi.org/10.1017/jog.2019.32>, 2019.
- Berthier, E., Vincent, C., Magnússon, E., Gunnlaugsson, Á. Þ., Pitte, P., Le Meur, E., Masiokas, M., Ruiz, L., Pálsson, F., Belart, J. M. C., and Wagnon, P.: Glacier topography and elevation changes derived from Pléiades sub-meter stereo images, *Cryosphere*, 8(6), 2275–2291, <https://doi.org/10.5194/tc-8-2275-2014>, 2014.
- 905 Berthier, E., Cabot, V., Vincent, C., and Six, D.: Decadal region-wide and glacier-wide mass balances derived from multi-temporal ASTER satellite Digital Elevation Models. Validation over the Mont-Blanc area, *Front. Earth Sci.*, 4, <https://doi.org/10.3389/feart.2016.00063>, 2016.
- 910 Bhattacharya, A., Bolch, T., Mukherjee, K., King, O., Menounos, B., Kapitsa, V., Neckel, N., Yang, W., and Yao, T.: High Mountain Asian glacier response to climate revealed by multi-temporal satellite observations since the 1960s, *Nat. Commun.*, 12(1), 4133, <https://doi.org/10.1038/s41467-021-24180-y>, 2021.
- Bippus, G.: Characteristics of summer snow areas on glaciers observed by means of Landsat data, Ph. D. thesis, University of Innsbruck, Austria, 2011.
- 915 Bolch, T., Yao, T., Kang, S., Buchroithner, M. F., Scherer, D., Maussion, F., Huintjes, E., and Schneider, C.: A glacier inventory for the western Nyainqêntanglha Range and the Nam Co Basin, Tibet, and glacier changes 1976–2009, *Cryosphere*, 4(3), 419–433, <https://doi.org/10.5194/tc-4-419-2010>, 2010.
- Bolch, T., Kulkarni, A., Kääb, A., Huggel, C., Paul, F., Cogley, J. G., Frey, H., Kargel, J. S., Fujita, K., Scheel, M., Bajracharya, S., and Stoffel, M.: The state and fate of Himalayan glaciers, *Science*, 336(6079), 310–314, <https://doi.org/10.1126/science.1215828>, 2012.
- 920 Bolch, T., Rohrbach, N., Kutuzov, S., Robson, B. A., and Osmonov, A.: Occurrence, evolution and ice content of ice-debris complexes in the Ak-Shiirak, Central Tien Shan revealed by geophysical and remotely-sensed investigations: Ice-debris complexes in Ak-Shiirak, *Earth Surf. Process Landf.*, 44(1), 129–143, <https://doi.org/10.1002/esp.4487>, 2019.
- 925 Bolch, T., Yao, T., Bhattacharya, A., Hu, Y., King, O., Liu, L., Pronk, J. B., Rastner, P., and Zhang, G.: Earth observation to investigate occurrence, characteristics and changes of glaciers, glacial lakes and rock glaciers in the Poiqu River basin (central Himalaya), *Remote Sens.*, 14(8), 1927, <https://doi.org/10.3390/rs14081927>, 2022.



- 930 Braun, M. H., Malz, P., Sommer, C., Fariñas-Barahona, D., Sauter, T., Casassa, G., Soruco, A., Skvarca, P., and Seehaus, T. C.: Constraining glacier elevation and mass changes in South America, *Nat. Clim. Chang.*, 9(2), 130–136, <https://doi.org/10.1038/s41558-018-0375-7>, 2019.
- Brun, F., Berthier, E., Wagnon, P., Kääb, A., and Treichler, D.: A spatially resolved estimate of High Mountain Asia glacier mass balances from 2000 to 2016, *Nat. Geosci.*, 10(9), 668–673. <https://doi.org/10.1038/ngeo2999>, 2017.
- 935 Brun, F., Wagnon, P., Berthier, E., Jomelli, V., Maharjan, S. B., Shrestha, F., and Kraaijenbrink, P. D. A.: Heterogeneous influence of glacier morphology on the mass balance variability in High Mountain Asia, *J. Geophys. Res. Earth Surf.*, 2018JF004838, <https://doi.org/10.1029/2018JF004838>, 2019.
- Burns, P., and Nolin, A.: Using atmospherically-corrected Landsat imagery to measure glacier area change in the Cordillera Blanca, Peru from 1987 to 2010, *Remote Sens. Environ.*, 140, 165–178. <https://doi.org/10.1016/j.rse.2013.08.026>, 2014.
- 940 Caidong, C., and Sorteberg, A.: Modelled mass balance of Xibu glacier, Tibetan Plateau: sensitivity to climate change, *J. Glaciol.*, 56(196), 235–248. <https://doi.org/10.3189/002214310791968467>, 2010.
- Ciraci, E., Velicogna, I., and Sutterley, T.: Mass balance of Novaya Zemlya Archipelago, Russian High Arctic, using time-variable gravity from GRACE and altimetry data from ICESat and CryoSat-2, *Remote Sens.*, 10(11), 1817, <https://doi.org/10.3390/rs10111817>, 2018.
- 945 Clarke, G. K. C., Anslow, F. S., Jarosch, A. H., Radić, V., Menounos, B., Bolch, T., and Berthier, E.: Ice volume and subglacial topography for Western Canadian glaciers from mass balance fields, Thinning Rates, and a Bed Stress Model, *J. Clim.*, 26(12), 4282–4303, <https://doi.org/10.1175/JCLI-D-12-00513.1>, 2013.
- Cogley, G. J.: Geodetic and direct mass-balance measurements: Comparison and joint analysis, *Ann. Glaciol.*, 50(50), 96–100. <https://doi.org/10.3189/172756409787769744>, 2009.
- 950 Cogley, J. G., Hock, R., Rasmussen, L. A., Arendt, A. A., Bauder, A., Braithwaite, R. J., Jansson, P., Kaser, G., Möller, M., Nicholson, L., and Zemp, M.: Glossary of glacier mass balance and related terms, IHP-VII Technical Documents in Hydrology No. 86, IACS Contribution No. 2, UNESCO-IHP, Paris.
- Davaze, L., Rabatel, A., Dufour, A., Hugonnet, R., and Arnaud, Y.: Region-wide annual glacier surface mass balance for the European Alps from 2000 to 2016, *Front. Earth Sci.*, 8, 149, <https://doi.org/10.3389/feart.2020.00149>, 2020.
- 955 Dehecq, A., Millan, R., Berthier, E., Gourmelen, N., Trouve, E., and Vionnet, V.: Elevation changes inferred from TanDEM-X data over the Mont-Blanc area: Impact of the X-Band Interferometric Bias, *IEEE J. Sel. Top. Appl. Earth Obs.*, 9(8), 3870–3882, <https://doi.org/10.1109/JSTARS.2016.2581482>, 2016.
- 960 Dehecq, A., Gourmelen, N., Gardner, A. S., Brun, F., Goldberg, D., Nienow, P. W., Berthier, E., Vincent, C., Wagnon, P., and Trouvé, E.: Twenty-first century glacier slowdown driven by mass loss in High Mountain Asia, *Nat. Geosci.*, 12(1), 22–27, <https://doi.org/10.1038/s41561-018-0271-9>, 2019.
- Denzinger, F., Machguth, H., Barandun, M., Berthier, E., Girod, L., Kronenberg, M., Usabaliyev, R., and Hoelzle, M.: Geodetic mass balance of Abramov Glacier from 1975 to 2015, *J. Glaciol.*, 67(262), 331–342, <https://doi.org/10.1017/jog.2020.108>, 2021.
- 965 Deschamps-Berger, C., Gascoin, S., Berthier, E., Deems, J., Gutmann, E., Dehecq, A., Shean, D., and Dumont, M.: Snow depth mapping from stereo satellite imagery in mountainous terrain: evaluation using airborne laser-scanning data, *Cryosphere*, 14(9), 2925–2940, <https://doi.org/10.5194/tc-14-2925-2020>, 2020.
- Duan, K., Xu, B., and Wu, G.: Snow accumulation variability at altitude of 7010 m a.s.l. in Muztag Ata mountain in Pamir Plateau during 1958–2002, *J. Hydrol.*, 531, 912–918, <https://doi.org/10.1016/j.jhydrol.2015.10.013>, 2015.
- 970 Dussaillant, I., Berthier, E., Brun, F., Masiokas, M., Hugonnet, R., Favier, V., Rabatel, A., Pitte, P., and Ruiz, L.: Two decades of glacier mass loss along the Andes, *Nat. Geosci.*, 12(10), 802–808, <https://doi.org/10.1038/s41561-019-0432-5>, 2019.
- Falaschi, D., Rivera, A., Lo Vecchio Repetto, A., Moragues, S., Villalba, R., Rastner, P., Zeller, J., and Salcedo, A. P.: Evolution of surface characteristics of three debris-covered glaciers in the Patagonian Andes from 1958 to 2020, *Front. Earth Sci.*, 9, 671854, <https://doi.org/10.3389/feart.2021.671854>, 2021.
- 975 Falaschi, D., Berthier, E., Belart, J. M. C., Bravo, C., Castro, M., Durand, M., and Villalba, R.: Increased mass loss of glaciers in Volcán Domuyo (Argentinian Andes) between 1962 and 2020, revealed by aerial photos and satellite stereo imagery, *J. Glaciol.*, 1–17, <https://doi.org/10.1017/jog.2022.43>, 2022.
- 980 Farinotti, D., Immerzeel, W. W., de Kok, R. J., Quincey, D. J., and Dehecq, A.: Manifestations and mechanisms of the Karakoram glacier anomaly, *Nat. Geosci.*, 13(1), 8–16, <https://doi.org/10.1038/s41561-019-0513-5>, 2020.
- Fischer, M., Huss, M., Kummert, M., and Hoelzle, M.: Application and validation of long-range terrestrial laser scanning to monitor the mass balance of very small glaciers in the Swiss Alps, *Cryosphere*, 10(3), 1279–1295, <https://doi.org/10.5194/tc-10-1279-2016>, 2016.
- 985 Fujita, K., and Ageta, Y.: Effect of summer accumulation on glacier mass balance on the Tibetan Plateau revealed by mass-balance model, *J. Glaciol.*, 46(153), 244–252, <https://doi.org/10.3189/172756500781832945>, 2000.





- 990 Gardelle, J., Berthier, E., Arnaud, Y., and Kääb, A.: Region-wide glacier mass balances over the Pamir-Karakoram-Himalaya during 1999–2011, *Cryosphere*, 7(4), 1263–1286, <https://doi.org/10.5194/tc-7-1263-2013>, 2013.
- Girod, L., Nuth, C., Kääb, A., McNabb, R., and Galland, O.: MMASTER: Improved ASTER DEMs for elevation change monitoring, *Remote Sens.*, 9(7), 704, <https://doi.org/10.3390/rs9070704>, 2017.
- 995 Gorelick, N., Hancher, M., Dixon, M., Ilyushchenko, S., Thau, D., and Moore, R.: Google Earth Engine: Planetary-scale geospatial analysis for everyone, *Remote Sens. Environ.*, 202, 18–27, <https://doi.org/10.1016/j.rse.2017.06.031>, 2017.
- Guillet, G., King, O., Lv, M., Ghuffar, S., Benn, D., Quincey, D., and Bolch, T.: A regionally resolved inventory of High Mountain Asia surge-type glaciers, derived from a multi-factor remote sensing approach, *Cryosphere*, 16(2), 603–623, <https://doi.org/10.5194/tc-16-603-2022>, 2022.
- 1000 Gleyzes, M. A., Perret, L., Kubik, P.: Pléiades system architecture and main performances, in: *International Archives of the Photogrammetry, Remote Sensing and Spatial Information Sciences, Volume XXXIX-B1, XXII ISPRS Congress, Melbourne, Australia, 25 August – 01 September 2012*, 2012.
- Guo, Z., Wang, N., Kehrwald, N. M., Mao, R., Wu, H., Wu, Y., and Jiang, X.: Temporal and spatial changes in Western Himalayan firn line altitudes from 1998 to 2009, *Glob. Planet. Change*, 118, 97–105, <https://doi.org/10.1016/j.gloplacha.2014.03.012>, 2014.
- 1005 Hersbach, H., Bell, B., Berrisford, P., Hirahara, S., Horányi, A., Muñoz-Sabater, J., Nicolas, J., Peubey, C., Radu, R., Schepers, D., Simmons, A., Soci, C., Abdalla, S., Abellan, X., Balsamo, G., Bechtold, P., Biavati, G., Bidlot, J., Bonavita, M., ... Thépaut, J.: The ERA5 global reanalysis, *Q. J. R. Meteorol. Soc.*, 146(730), 1999–2049, <https://doi.org/10.1002/qj.3803>, 2020.
- Holzer, N., Vijay, S., Yao, T., Xu, B., Buchroithner, M., and Bolch, T.: Four decades of glacier variations at Muztag Ata (eastern Pamir): a multi-sensor study including Hexagon KH-9 and Pléiades data, *Cryosphere*, 9(6), 2071–2088, <https://doi.org/10.5194/tc-9-2071-2015>, 2015.
- Hou, A. Y., Kakar, R. K., Neeck, S., Azarbarzin, A. A., Kummerow, C. D., Kojima, M., Oki, R., Nakamura, K., and Iguchi, T.: The Global Precipitation Measurement Mission, *Bull Am Meteorol Soc.*, 95(5), 701–722, <https://doi.org/10.1175/BAMS-D-13-00164.1>, 2014.
- 1015 Huang, L., Li, Z., Tian, B., Chen, Q., and Zhou, J.: Monitoring glacier zones and snow/firn line changes in the Qinghai–Tibetan Plateau using C-band SAR imagery, *Remote Sens. Environ.*, 137, 17–30, <https://doi.org/10.1016/j.rse.2013.05.016>, 2013.
- Huang, L., Hock, R., Li, X., Bolch, T., Yang, K., Wang, N., Yao, T., Zhou, J., Dou, C., and Li, Z.: Winter accumulation drives the spatial variations in glacier mass balance in High Mountain Asia, *Sci. Bull.*, S2095927322003644, <https://doi.org/10.1016/j.scib.2022.08.019>, 2012.
- 1020 Huintjes, E., Sauter, T., Schröter, B., Maussion, F., Yang, W., Kropáček, J., Buchroithner, M., Scherer, D., Kang, S., and Schneider, C.: Evaluation of a coupled snow and energy balance model for Zhadang Glacier, Tibetan Plateau, using glaciological measurements and time-lapse photography, *Arct. Antarct. Alp. Res.*, 47(3), 573–590, <https://doi.org/10.1657/AAAR0014-073>, 2015.
- 1025 Huffman, G. J., Bolvin, D. T., Braithwaite, D., Hsu, K., Joyce, R., Xie, P., and Yoo, S. H.: NASA global precipitation measurement (GPM) integrated multi-satellite retrievals for GPM (IMERG). Algorithm Theoretical Basis Document (ATBD) Version, 4(26), 2015.
- Huss, M.: Density assumptions for converting geodetic glacier volume change to mass change, *Cryosphere*, 7(3), 877–887, <https://doi.org/10.5194/tc-7-877-2013>, 2013.
- 1030 Huss, M., Sold, L., Hoelzle, M., Stokvis, M., Salzmann, N., Farinotti, D., and Zemp, M.: Towards remote monitoring of sub-seasonal glacier mass balance, *Ann. Glaciol.*, 54(63), 75–83, <https://doi.org/10.3189/2013AoG63A427>, 2013.
- Hugonnet, R., McNabb, R., Berthier, E., Menounos, B., Nuth, C., Girod, L., Farinotti, D., Huss, M., Dussaillant, I., Brun, F., and Kääb, A.: Accelerated global glacier mass loss in the early twenty-first century, *Nature*, 592(7856), 726–731, <https://doi.org/10.1038/s41586-021-03436-z>, 2021.
- 1035 Hugonnet, R., Brun, F., Berthier, E., Dehecq, A., Mannerfelt, E. S., Eckert, N., and Farinotti, D.: Uncertainty analysis of digital elevation models by spatial inference from stable terrain, *IEEE J. Sel. Top. Appl. Earth Obs. Remote Sens.*, 1–17, <https://doi.org/10.1109/JSTARS.2022.3188922>, 2022.
- 1040 Immerzeel, W. W., Lutz, A. F., Andrade, M. et al.: Importance and vulnerability of the world’s water towers, *Nature*, 577, 364–369, <https://doi.org/10.1038/s41586-019-1822-y>, 2020.
- Kääb, A., Treichler, D., Nuth, C., and Berthier, E.: Brief Communication: Contending estimates of 2003–2008 glacier mass balance over the Pamir–Karakoram–Himalaya, *Cryosphere*, 9(2), 557–564, <https://doi.org/10.5194/tc-9-557-2015>, 2015.
- 1045 Kääb, A., Winsvold, S., Altena, B., Nuth, C., Nagler, T., and Wuite, J.: Glacier remote sensing using Sentinel-2. Part I: radiometric and geometric performance, and application to ice velocity, *Remote Sens.*, 8(7), 598, <https://doi.org/10.3390/rs8070598>, 2016.



- Kang, S., Chen, F., Gao, T., Zhang, Y., Yang, W., Yu, W., and Yao, T.: Early onset of rainy season suppresses glacier melt: A case study on Zhadang glacier, Tibetan Plateau, *J. Glaciol.*, 55(192), 755–758, <https://doi.org/10.3189/002214309789470978>, 2009.
- 1050 King, O., Bhattacharya, A., Bhambri, R., and Bolch, T.: Glacial lakes exacerbate Himalayan glacier mass loss, *Sci. Rep.*, 9(1), 18145, <https://doi.org/10.1038/s41598-019-53733-x>, 2019.
- King, O., Bhattacharya, A., and Bolch, T.: The presence and influence of glacier surging around the Geladandong ice caps, North East Tibetan Plateau, *Adv. Clim. Chang. Res.*, 12(3), 299–312, <https://doi.org/10.1016/j.accre.2021.05.001>, 2021.
- 1055 Koblet, T., Gärtner-Roer, I., Zemp, M., Jansson, P., Thee, P., Haeberli, W., and Holmlund, P.: Reanalysis of multi-temporal aerial images of Storglaciären, Sweden (1959-99) - Part 1: determination of length, area, and volume changes, *Cryosphere*, 4(3), 333–343, <https://doi.org/10.5194/tc-4-333-2010>, 2010.
- Li, G., and Lin, H.: Recent decadal glacier mass balances over the Western Nyainqêntanglha Mountains and the increase in their melting contribution to Nam Co Lake measured by differential bistatic SAR interferometry, *Glob. Planet. Change*, 149, 177–190, <https://doi.org/10.1016/j.gloplacha.2016.12.018>, 2017.
- 1060 Lin, Q., Chen, J., Chen, D., Wang, X., Li, W., and Scherer, D.: Impacts of bias-corrected ERA5 initial snow depth on dynamical downscaling simulations for the Tibetan Plateau, *J. Geophys. Res. Atmos.*, 126(23), <https://doi.org/10.1029/2021JD035625>, 2021.
- 1065 Liang, Q., Wang, N., Yang, X., Chen, A., Hua, T., Li, Z., and Yang, D.: The eastern limit of ‘Kunlun-Pamir-Karakoram Anomaly’ reflected by changes in glacier area and surface elevation, *J. Glaciol.*, 68(272), 1167–1176, <https://doi.org/10.1017/jog.2022.30>, 2022.
- Luo, W., Zhang, G., Chen, W., and Xu, F.: Response of glacial lakes to glacier and climate changes in the Western Nyainqêntanglha range, *Sci. Total Environ.*, 735, 139607, <https://doi.org/10.1016/j.scitotenv.2020.139607>, 2020.
- 1070 Lv, M., Quincey, D. J., Guo, H., King, O., Liu, G., Yan, S., Lu, X., and Ruan, Z.: Examining geodetic glacier mass balance in the eastern Pamir transition zone, *J. Glaciol.*, 66(260), 927–937, <https://doi.org/10.1017/jog.2020.54>, 2020.
- Maussion, F., Scherer, D., Mölg, T., Collier, E., Curio, J., and Finkelnburg, R.: Precipitation seasonality and variability over the Tibetan Plateau as resolved by the High Asia Reanalysis, *J. Clim.*, 27(5), 1910–1927, <https://doi.org/10.1175/JCLI-D-13-00282.1>, 2014.
- 1075 Maussion, F., Butenko, A., Champollion, N., Dusch, M., Eis, J., Fourteau, K., Gregor, P., Jarosch, A. H., Landmann, J., Oesterle, F., Recinos, B., Rothenpieler, T., Vlug, A., Wild, C. T., and Marzeion, B.: The Open Global Glacier Model (OGGM) v1.1., *Geosci. Model. Dev.*, 12(3), 909–931, <https://doi.org/10.5194/gmd-12-909-2019>, 2019.
- 1080 McNabb, R., Nuth, C., Kääh, A., and Girod, L.: Sensitivity of glacier volume change estimation to DEM void interpolation, *Cryosphere*, 13(3), 895–910, <https://doi.org/10.5194/tc-13-895-2019>, 2019.
- Miles, E., McCarthy, M., Dehecq, A., Kneib, M., Fugger, S., and Pellicciotti, F.: Health and sustainability of glaciers in High Mountain Asia, *Nat. Commun.*, 12(1), 2868, <https://doi.org/10.1038/s41467-021-23073-4>, 2021.
- 1085 Mölg, T., Maussion, F., Yang, W., and Scherer, D.: The footprint of Asian monsoon dynamics in the mass and energy balance of a Tibetan glacier, *Cryosphere*, 6(6), 1445–1461, <https://doi.org/10.5194/tc-6-1445-2012>, 2012.
- Mölg, T., Maussion, F., and Scherer, D.: Mid-latitude westerlies as a driver of glacier variability in monsoonal High Asia, *Nat. Clim. Chang.*, 4(1), 68–73, <https://doi.org/10.1038/nclimate2055>, 2014.
- Mukherjee, K., Menounos, B., Shea, J., Mortezapour, M., Ednie, M., and Demuth, M. N.: Evaluation of surface mass-balance records using geodetic data and physically-based modelling, Place and Peyto glaciers, western Canada, *J. Glaciol.*, 1–18, <https://doi.org/10.1017/jog.2022.83>, 2022.
- 1090 Muñoz-Sabater, J., Dutra, E., Agustí-Panareda, A., Albergel, C., Arduini, G., Balsamo, G., Boussetta, S., Choulga, M., Harrigan, S., Hersbach, H., Martens, B., Miralles, D. G., Piles, M., Rodríguez-Fernández, N. J., Zsoter, E., Buontempo, C., and Thépaut, J.-N.: ERA5-Land: A state-of-the-art global reanalysis dataset for land applications, *Earth System Science Data*, 13(9), 4349–4383, <https://doi.org/10.5194/essd-13-4349-2021>, 2021.
- 1095 Nuth, C., and Kääh, A.: Co-registration and bias corrections of satellite elevation data sets for quantifying glacier thickness change, *Cryosphere*, 5(1), 271–290, <https://doi.org/10.5194/tc-5-271-2011>, 2011.
- Otsu, N.: A Threshold Selection Method from Gray-Level Histograms, *IEEE Trans. Syst. Man Cybern. Syst.*, 9(1), 62–66, <https://doi.org/10.1109/TSMC.1979.4310076>, 1979.
- 1100 Paul, F., Bolch, T., Kääh, A., et al.: The glaciers climate change initiative: methods for creating glacier area, elevation change and velocity products, *Remote Sens. Environ.*, 162, 408–426, <https://doi.org/10.1016/j.rse.2013.07.043>, 2015.
- Pelto, B. M., Menounos, B., and Marshall, S. J.: Multi-year evaluation of airborne geodetic surveys to estimate seasonal mass balance, Columbia and Rocky Mountains, Canada, *Cryosphere*, 13(6), 1709–1727, <https://doi.org/10.5194/tc-13-1709-2019>, 2019.



- 1105 Racoviteanu, A. E., Rittger, K., and Armstrong, R.: An automated approach for estimating snowline altitudes in the Karakoram and Eastern Himalaya from Remote Sensing, *Front. Earth Sci.*, 7, 220, <https://doi.org/10.3389/feart.2019.00220>, 2019.
- Rastner, P., Prinz, R., Notarnicola, C., Nicholson, L., Sailer, R., Schwaizer, G., and Paul, F.: On the automated mapping of snow cover on glaciers and calculation of snow line altitudes from multi-temporal Landsat data, *Remote Sens.*, 11(12), 1410, <https://doi.org/10.3390/rs11121410>, 2019.
- 1110 Ren, S., Menenti, M., Jia, L., Zhang, J., Zhang, J., and Li, X.: Glacier mass balance in the Nyainqêntanglha Mountains between 2000 and 2017 retrieved from ZiYuan-3 stereo images and the SRTM DEM, *Remote Sens.*, 12(5), 864, <https://doi.org/10.3390/rs12050864>, 2020.
- RGI Consortium: Randolph Glacier Inventory—A dataset of global glacier outlines, Version 6 [data set], <https://doi.org/10.7265/4M1F-GD79>, 2017.
- 1115 Sakai, A., Nuimura, T., Fujita, K., Takenaka, S., Nagai, H., and Lamsal, D.: Climate regime of Asian glaciers revealed by GAMDAM glacier inventory, *Cryosphere*, 9(3), 865–880, <https://doi.org/10.5194/tc-9-865-2015>, 2015.
- Sakai, A., and Fujita, K.: Contrasting glacier responses to recent climate change in high-mountain Asia, *Sci. Rep.*, 7(1), 13717, <https://doi.org/10.1038/s41598-017-14256-5>, 2017.
- 1120 Scherler, D., Wulf, H., and Gorelick, N.: Global assessment of supraglacial debris-cover extents, *Geophys. Res. Lett.*, 45(21), 11,798–11,805, <https://doi.org/10.1029/2018GL080158>, 2018.
- Seong, Y. B., Owen, L. A., Yi, C., Finkel, R. C., and Schoenbohm, L.: Geomorphology of anomalously high glaciated mountains at the northwestern end of Tibet: Muztag Ata and Kongur Shan, *Geomorphology*, 103(2), 227–250, <https://doi.org/10.1016/j.geomorph.2008.04.025>, 2009.
- 1125 Shangguan, D., Liu, S., Ding, Y., Ding, L., Xiong, L., Cai, D., Li, G., Lu, A., Zhang, S., and Zhang, Y.: Monitoring the glacier changes in the Muztag Ata and Konggur mountains, east Pamirs, based on Chinese Glacier Inventory and recent satellite imagery, *Ann. Glaciol.*, 43, 79–85, <https://doi.org/10.3189/172756406781812393>, 2006.
- 1130 Shean, D. E., Alexandrov, O., Moratto, Z. M., Smith, B. E., Joughin, I. R., Porter, C., and Morin, P.: An automated, open-source pipeline for mass production of digital elevation models (DEMs) from very-high-resolution commercial stereo satellite imagery, *ISPRS J. Photogramm. Remote Sens.*, 116, 101–117, <https://doi.org/10.1016/j.isprsjprs.2016.03.012>, 2016.
- 1135 Shean, D. E., Bhushan, S., Montesano, P., Rounce, D. R., Arendt, A., and Osmanoglu, B.: A systematic, regional assessment of High Mountain Asia glacier mass balance, *Front. Earth Sci.*, 7, 363, <https://doi.org/10.3389/feart.2019.00363>, 2020.
- Shi, J., and Menenti, M.: Monitoring recent variations of the movements on the polythermal glaciers -a case study in the Nyainqêntanglha Mountains, in: 2013 IEEE International Geoscience and Remote Sensing Symposium - IGARSS, 2013, 3622–3625, <https://doi.org/10.1109/IGARSS.2013.6723614>, 2013.
- 1140 Sommer, C., Malz, P., Seehaus, T. C., Lippl, S., Zemp, M., and Braun, M. H.: Rapid glacier retreat and downwasting throughout the European Alps in the early 21st century, *Nat. Commun.*, 11(1), 3209, <https://doi.org/10.1038/s41467-020-16818-0>, 2020.
- Vishwakarma, B. D., Ramsankaran, R., Azam, Mohd. F. et al.: Challenges in understanding the variability of the cryosphere in the Himalaya and its impact on regional water Resources, *Front. Water*, 4, 909246, <https://doi.org/10.3389/frwa.2022.909246>, 2022.
- 1145 Wagnon, P., Brun, F., Khadka, A., Berthier, E., Shrestha, D., Vincent, C., Arnaud, Y., Six, D., Dehecq, A., Ménégoz, M., and Jomelli, V.: Reanalysing the 2007–19 glaciological mass-balance series of Mera Glacier, Nepal, Central Himalaya, using geodetic mass balance, *J. Glaciol.*, 67(261), 117–125, <https://doi.org/10.1017/jog.2020.88>, 2021.
- 1150 Wang, S., Liu, J., Pritchard, H. D., Ke, L., Qiao, X., Zhang, J., Xiao, W., and Zhou, Y.: Characterizing four decades of accelerated glacial mass loss in the West Nyainqêntanglha Range of the Tibetan Plateau [preprint], *Hydro. Earth Syst. Sci.*, <https://doi.org/10.5194/hess-2022-179>, 2022.
- Wang, X., Tolksdorf, V., Otto, M., and Scherer, D.: WRF-based dynamical downscaling of ERA5 reanalysis data for High Mountain Asia: towards a new version of the High Asia Refined analysis, *Int. J. Climatol.*, 41(1), 743–762, <https://doi.org/10.1002/joc.6686>, 2021.
- 1155 WGMS: Global Glacier Change Bulletin No. 4 (2018–2019), edited by: Zemp, M., Nussbaumer, S. U., Gärtner-Roer, I., Bannwart, J., Paul, F., and Hoelzle, M., ISC(WDS)/IUGG(IACS)/UNEP/UNESCO/WMO, World Glacier Monitoring Service, Zurich, Switzerland, <https://doi.org/10.5904/wgms-fog-2021-05>, 2021.
- Wortmann, M., Bolch, T., Menz, C., Tong, J., and Krysanova, V.: Comparison and correction of high-mountain precipitation data based on glacio-hydrological modeling in the Tarim River headwaters (High Asia), *J. Hydrometeorol.*, 19(5), 777–801, <https://doi.org/10.1175/JHM-D-17-0106.1>, 2018.
- 1160 Wu, K., Liu, S., Guo, W., Wei, J., Xu, J., Bao, W., and Yao, X.: Glacier change in the western Nyainqêntanglha Range, Tibetan Plateau using historical maps and Landsat imagery: 1970–2014, *J. Mt. Sci.*, 13(8), 1358–1374, <https://doi.org/10.1007/s11629-016-3997-0>, 2016.



- 1165 Wu, K., Liu, S., Zhu, Y., Xie, F., Gao, Y., Qi, M., Miao, W., Duan, S., Han, F., and Grünwald, R.: Monitoring the surface elevation changes of a monsoon temperate glacier with repeated UAV surveys, Mainri Mountains, China, *Remote Sens.*, 14(9), 2229, <https://doi.org/10.3390/rs14092229>, 2022.
- Xu, C., Li, Z., Wang, P., Anjum, M. N., Li, H., and Wang, F.: Detailed comparison of glaciological and geodetic mass balances for Urumqi Glacier No.1, eastern Tien Shan, China, from 1981 to 2015, *Cold Reg Sci Technol.*, 155, 137–148, <https://doi.org/10.1016/j.coldregions.2018.08.006>, 2018.
- 1170 Yan, S., Guo, H., Liu, G., and Ruan, Z.: Mountain glacier displacement estimation using a DEM-assisted offset tracking method with ALOS/PALSAR data, *Remote Sens. Lett.*, 4(5), 494–503, <https://doi.org/10.1080/2150704X.2012.754561>, 2013.
- Yang, H., Yan, S., Liu, G., and Ruan, Z.: Fluctuations and movements of the Kuksai Glacier, western China, derived from Landsat image sequences, *J. Appl. Remote. Sens.*, 8(1), 084599, <https://doi.org/10.1117/1.JRS.8.084599>, 2013.
- 1175 Yao, T.: Map of glaciers and lakes on the Tibetan Plateau and adjoining regions 1:2 000 000, Xian Cartographic Publishing House, 2008.
- Yao, T., Li, Z., Yang, W., Guo, X., Zhu, L., Kang, S., Wu, Y., and Yu, W.: Glacial distribution and mass balance in the Yarlung Zangbo River and its influence on lakes, *Chinese Science Bulletin*, 55(20), 2072–2078, <https://doi.org/10.1007/s11434-010-3213-5>, 2010.
- Yao, T., Thompson, L., Yang, W., Yu, W., Gao, Y., Guo, X., Yang, X., Duan, K., Zhao, H., Xu, B., Pu, J., Lu, A., Xiang, Y., Kattel, D. B., and Joswiak, D.: Different glacier status with atmospheric circulations in Tibetan Plateau and surroundings, *Nat. Clim. Chang.*, 2(9), 663–667, <https://doi.org/10.1038/nclimate1580>, 2012.
- 1185 Yao, T., Bolch, T., Chen, D., Gao, J., Immerzeel, W., Piao, S., Su, F., Thompson, L., Wada, Y., Wang, L., Wang, T., Wu, G., Xu, B., Yang, W., Zhang, G., and Zhao, P.: The imbalance of the Asian water tower, *Nat. Rev. Phys.*, <https://doi.org/10.1038/s43017-022-00299-4>, 2022.
- Zemp, M., Thibert, E., Huss, M., Stumm, D., Rolstad Denby, C., Nuth, C., Nussbaumer, S. U., Moholdt, G., Mercer, A., Mayer, C., Joerg, P. C., Jansson, P., Hynes, B., Fischer, A., Escher-Vetter, H., Elvehøy, H., and Andreassen, L. M.: Reanalysing glacier mass balance measurement series, *Cryosphere*, 7(4), 1227–1245, <https://doi.org/10.5194/tc-7-1227-2013>, 2013.
- 1190 Zemp, M., Frey, H., Gärtner-Roer, I.: Historically unprecedented global glacier decline in the early 21st century, *J. Glaciol.*, 61(228), 745–762, <https://doi.org/10.3189/2015Jog15J017>, 2015.
- Zhang, G., Kang, S., Fujita, K., Huintjes, E., Xu, J., Yamazaki, T., Haginoya, S., Wei, Y., Scherer, D., Schneider, C., and Yao, T.: Energy and mass balance of Zhadang glacier surface, central Tibetan Plateau, *J. Glaciol.*, 59(213), 137–148, <https://doi.org/10.3189/2013Jog12J152>, 2013.
- 1195 Zhang, Q., and Zhang, G.: Glacier elevation changes in the western Nyainqêntanglha Range of the Tibetan Plateau as observed by TerraSAR-X/TanDEM-X images, *Remote Sens. Lett.*, 8(12), 1142–1151, <https://doi.org/10.1080/2150704X.2017.1362123>, 2017.
- 1200 Zhang, Z., Liu, S., Wei, J., Xu, J., Guo, W., Bao, W., and Jiang, Z.: Mass change of glaciers in Muztag Ata–Kongur Tagh, eastern Pamir, China from 1971/76 to 2013/14 as derived from remote sensing data, *PLoS One*, 11(1), e0147327, <https://doi.org/10.1371/journal.pone.0147327>, 2016.
- Zhou, J., Li, Z., and Guo, W.: Estimation and analysis of the surface velocity field of mountain glaciers in Muztag Ata using satellite SAR data, *Environ. Earth Sci.*, 71(8), 3581–3592, <https://doi.org/10.1007/s12665-013-2749-5>, 2014.
- 1205 Zhou, Y., Li, Z., Li, J., Zhao, R., and Ding, X.: Glacier mass balance in the Qinghai–Tibet Plateau and its surroundings from the mid-1970s to 2000 based on Hexagon KH-9 and SRTM DEMs, *Remote Sens. Environ.*, 210, 96–112, <https://doi.org/10.1016/j.rse.2018.03.020>, 2018.
- Zhu, M., Yao, T., Yang, W., Maussion, F., Huintjes, E., and Li, S.: Energy- and mass-balance comparison between Zhadang and Parlung No. 4 glaciers on the Tibetan Plateau, *J. Glaciol.*, 61(227), 595–607, <https://doi.org/10.3189/2015Jog14J206>, 2015.
- 1210 Zhu, M., Yao, T., Yang, W., Xu, B., Wu, G., Wang, X., and Xie, Y.: Reconstruction of the mass balance of Muztag Ata No. 15 glacier, eastern Pamir, and its climatic drivers, *J. Glaciol.*, 64(244), 259–274, <https://doi.org/10.1017/jog.2018.16>, 2018a.
- 1215 Zhu, M., Yao, T., Yang, W., Xu, B., Wu, G., and Wang, X.: Differences in mass balance behavior for three glaciers from different climatic regions on the Tibetan Plateau, *Clim. Dyn.*, 50(9–10), 3457–3484, <https://doi.org/10.1007/s00382-017-3817-4>, 2018b.